Visualizing in situ translational activity for identifying and sorting slow-growing archaeal–bacterial consortia

Roland Hatzenpichler[a,1], Stephanie A. Connon[a], Danielle Goudeau[b], Rex R. Malmstrom[b], Tanja Woyke[b], and Victoria J. Orphan[a,1]

[a]Division of Geological and Planetary Sciences, California Institute of Technology, Pasadena, CA 91125; and [b]Joint Genome Institute, Department of Energy, Walnut Creek, CA 94598

Edited by Edward F. DeLong, University of Hawaii at Manoa, Honolulu, HI, and approved May 25, 2016 (received for review March 7, 2016)

To understand the biogeochemical roles of microorganisms in the environment, it is important to determine when and under which conditions they are metabolically active. Bioorthogonal noncanonical amino acid tagging (BONCAT) can reveal active cells by tracking the incorporation of synthetic amino acids into newly synthesized proteins. The phylogenetic identity of translationally active cells can be determined by combining BONCAT with rRNA-targeted fluorescence in situ hybridization (BONCAT-FISH). In theory, BONCAT-labeled cells could be isolated with fluorescence-activated cell sorting (BONCAT-FACS) for subsequent genetic analyses. Here, in the first application, to our knowledge, of BONCAT-FISH and BONCAT-FACS within an environmental context, we probe the translational activity of microbial consortia catalyzing the anaerobic oxidation of methane (AOM), a dominant sink of methane in the ocean. These consortia, which typically are composed of anaerobic methane-oxidizing archaea (ANME) and sulfate-reducing bacteria, have been difficult to study due to their slow in situ growth rates, and fundamental questions remain about their ecology and diversity of interactions occurring between ANME and associated partners. Our activity-correlated analyses of >16,400 microbial aggregates provide the first evidence, to our knowledge, that AOM consortia affiliated with all five major ANME clades are concurrently active under controlled conditions. Surprisingly, sorting of individual BONCAT-labeled consortia followed by whole-genome amplification and 16S rRNA gene sequencing revealed previously unrecognized interactions of ANME with members of the poorly understood phylum *Verrucomicrobia*. This finding, together with our observation that ANME-associated *Verrucomicrobia* are found in a variety of geographically distinct methane seep environments, suggests a broader range of symbiotic relationships within AOM consortia than previously thought.

activity-based cell sorting | BONCAT | click chemistry | ecophysiology | single-cell microbiology

Some of the most important goals of environmental microbiology are to understand the physiology, niche differentiation, and activities of microorganisms in the context of their habitat. Studies focusing on the mere presence of a cell or gene in a sample can only provide limited information about the metabolic capabilities of an organism. Coupling the identification of an uncultured microbe with its in situ activity thus has been referred to as the "Holy Grail" of microbial ecology (1). Although bulk techniques, such as metatranscriptomics and metaproteomics or stable isotope probing targeted at DNA, RNA, or proteins, have provided us with exciting new insights into microbial ecophysiology (1–3), they cannot resolve cellular activities on the micrometer scale. The combination of rRNA-targeted fluorescence in situ hybridization (FISH) with single-cell resolving stable isotope analysis offers a direct, targeted approach for detailed investigations of microbial structure–function relationships (4, 5).

Currently, three broadly applicable approaches for studying the in situ anabolic activity of individual cells are available: microautoradiography (MAR) (6), secondary ion mass spectroscopy (SIMS and nanoSIMS) (7), and Raman microspectroscopy (Raman) (8). Each of these techniques has technical challenges or limited instrument availability that have slowed their wide adoption in the field (1, 5, 9). MAR and SIMS are also destructive methods that cannot be combined with downstream analysis such as cell sorting, subculturing, or genomic sequencing. Another problem is that many biomolecules are prohibitively expensive or even unavailable in their isotopically labeled form. A universally applicable approach that circumvents these limitations was recently established by combining the general labeling of active cells via heavy water with their subsequent identification via FISH and sorting via Raman-coupled optical tweezers (10). Complementary to detecting anabolic activity via isotope labeling, a fluorescence technique based on the visualization of bacterial reductase activity via redox sensing (Redox sensor green) has been described (11, 12). The general applicability and exact mechanism of this proprietary staining method are, however, unknown.

An alternative approach for studying microbial ecophysiology that does not depend on isotopes is labeling active cells via chemically modifiable analogs of biomolecules (9, 13, 14). Bioorthogonal noncanonical amino acid tagging (BONCAT) is a nondestructive technique first applied in neurobiology (15, 16). Last year, BONCAT was adapted for the study of uncultured

Significance

One of the biggest challenges in environmental microbiology is to determine the activity of uncultured cells directly in their habitat. We report on the application of bioorthogonal noncanonical amino acid tagging (BONCAT), a high-throughput approach to detecting protein synthesis in individual cells by fluorescence staining, on deep-sea methane seep sediments. By combining BONCAT with fluorescence in situ hybridization, we visualized active archaeal–bacterial consortia catalyzing the anaerobic oxidation of methane. We further developed a novel approach that combines BONCAT with fluorescence-activated cell sorting (FACS) to separate translationally active cells from complex samples. BONCAT-FACS enabled us to directly link the identities of anaerobic methane-oxidizing archaea with their partner bacteria for individual active consortia, uncovering previously unknown interactions between these archaea and *Verrucomicrobia*.

Author contributions: R.H. and V.J.O. designed research; R.H., S.A.C., and D.G. performed research; R.R.M., T.W., and V.J.O. contributed new reagents/analytic tools; R.H. and D.G. analyzed data; and R.H. and V.J.O. wrote the paper with input from all authors.

The authors declare no conflict of interest.

This article is a PNAS Direct Submission.

Freely available online through the PNAS open access option.

Data deposition: The sequences reported in this paper have been deposited in the National Center for Biotechnology Information GenBank database (accession nos. KT945170–KT945234 and KU564217–KU564240) and Sequence Read Archive (accession no. SRP066109).

[1]To whom correspondence may be addressed. Email: hatzenpichler@caltech.edu or vorphan@gps.caltech.edu.

This article contains supporting information online at www.pnas.org/lookup/suppl/doi:10.1073/pnas.1603757113/-/DCSupplemental.

archaea and bacteria within environmental samples (9, 14). BONCAT depends on the addition of a bioorthogonal (non-interacting with cellular functionalities) synthetic (noncanonical) amino acid to a sample. After its uptake (the exact process is currently unknown), the amino acid is able to exploit the substrate promiscuity of specific amino acyl tRNA synthetases, the enzymes catalyzing the esterification of amino acids with their respective cognate tRNAs, to get incorporated into de novo peptides (17). Protein synthesis-active cells can, in the following, be visualized via a highly selective click chemistry-mediated labeling reaction that conjugates a modified fluorescence dye to a chemical reporter group (an azide or alkyne) of the bioorthogonal amino acid (Fig. 1*A*). Although a wide range of synthetic amino acids exists, only a small number are able to exploit the natural translational machinery without the need for genetic modification of the cell (18). To date, the L-methionine (Met) surrogates L-azidohomoalanine (AHA) and L-homopropargylglycine (HPG) (17) have found the widest application (e.g., refs. 16 and 19–24). In a proof-of-principle investigation, BONCAT was applied to environmental samples and found to be generally applicable to uncultured archaea and bacteria (9, 14). BONCAT has been demonstrated to correlate well with other, independent proxies of cellular growth, i.e., the incorporation of isotopically labeled compounds as detected by nanoscale SIMS, $^{15}NH_4^+$ (9), and MAR, [^{35}S]Met (14). In addition, a protocol for the concomitant taxonomic identification of translationally active cells via rRNA-targeted FISH (i.e., BONCAT-FISH) was recently developed (9) (Fig. 1 *A* and *B*).

In this study, we applied HPG to deep-sea methane seep sediments in which the sulfate-coupled anaerobic oxidation of methane (AOM) is occurring. AOM accounts for the removal of ∼80% of the methane released from ocean sediments (>400 Gt·y^{-1}) and is a key process in the biogeochemical cycling of this highly potent greenhouse gas (25). In marine seeps, AOM is predominantly catalyzed by a symbiosis of anaerobic methane-oxidizing euryarchaeotes (ANME) with sulfate-reducing bacteria (SRB), which form consortia of varying cell numbers (∼10 to ∼10^5 cells) and morphology (7, 26). Their syntrophic partnership is hypothesized to be mediated by direct electron transfer (27–29) and/or diffusible intermediates (30, 31).

Several different ANME clades (referred to as ANME-1a, -1b, -2a, -2b, -2c, and -3) have been observed to aggregate with different representatives of SRB (particularly members of the *Desulfosarcina*, *Desulfococcus*, and *Desulfobulbus* genera), with multiple ANME–SRB consortia of different taxonomies commonly coexisting in seep sediments without apparent competitive exclusion of one another. The potential for ecological niche partitioning within these highly diverse yet seemingly functionally redundant associations is not well understood. Previously, it was demonstrated that temperature (32), methane partial pressure (32), concentrations of sulfate (33, 34) and sulfide (34), and the availability of nitrogen (35, 36) may influence distribution and activity of AOM consortia. In addition, ANME-community structure can vary dramatically between geographically proximate sites as well as distinct sediment layers (37, 38). Whether different ANME subgroups in a given sample show variable activities depending on specific physicochemical or ecological conditions or are all metabolically active at a given time is unknown. In addition to sulfate reducers, other bacterial lineages,

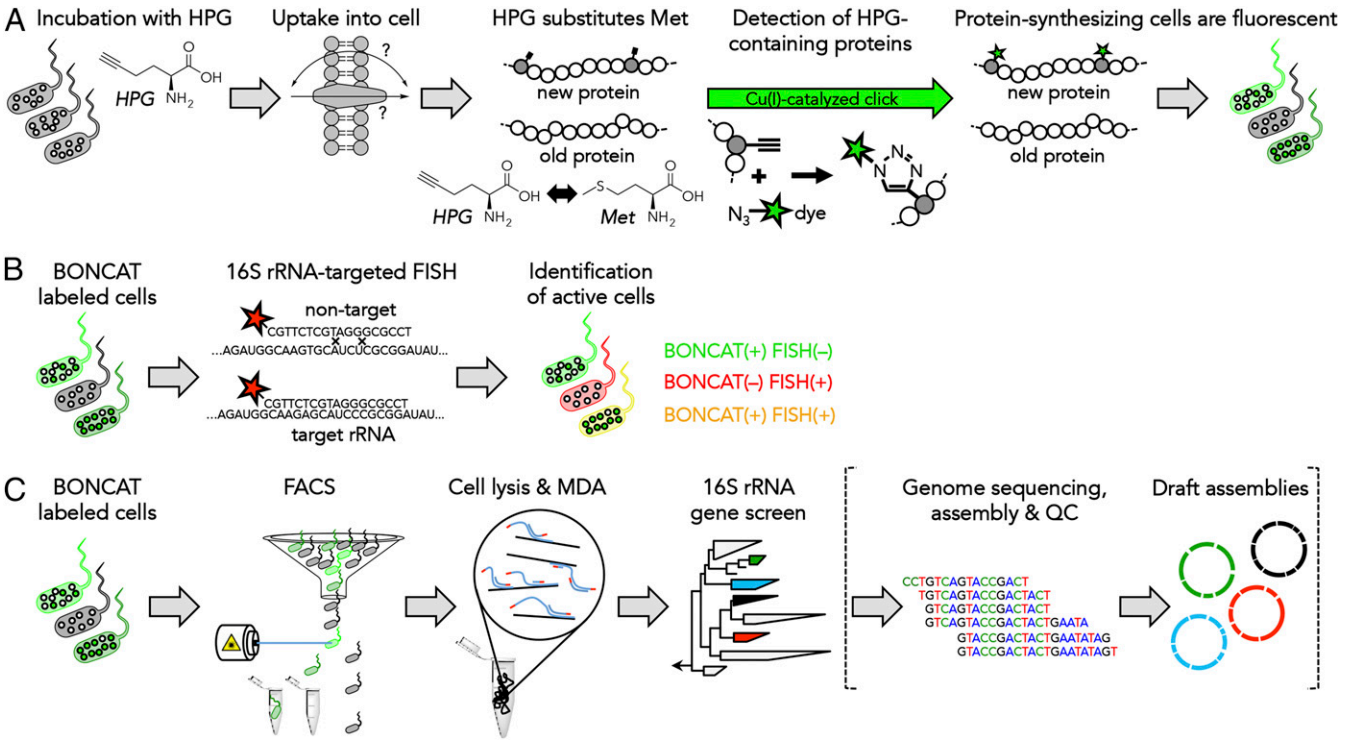

Fig. 1. Concept for the visualization, identification, and sorting of translationally active cells. (*A*) The bioorthogonal amino acid HPG is added to an environmental sample, which is then incubated under in situ conditions. After HPG has entered the cell, the exact process of which is currently unknown, it competes with Met for incorporation into newly made peptides. HPG-containing proteins are then fluorescently labeled via a Cu(I)-catalyzed azide–alkyne click reaction, thus marking cells that have undergone protein synthesis during time of incubation. (*B*) Next, rRNA-targeted FISH is performed to taxonomically identify anabolically active cells. In this example, the yellow cell is detected via both BONCAT and FISH, whereas the other two were either not translationally active (red cell) or are taxonomically unidentified but active (green cell). (*C*) Individual labeled cells or consortia can be separated using FACS. Cells are lysed and their genomes amplified using MDA. The resulting amplified genomes are taxonomically screened via amplification and sequencing of the V4 region of the 16S rRNA gene. This information may then guide the selection of cells or consortia for genomic sequencing.

including members of the alpha-, beta-, gamma-, and epsilon-proteobacteria, have been observed to form physical associations with ANME (39, 40). The metabolic interactions underlying these relationships are, however, yet to be determined.

Our study represents, to our knowledge, the first research application of BONCAT-FISH in environmental microbiology. We tested the influence of methane on the metabolic activity (protein synthesis) of diverse AOM consortia in three sediment samples from two geographically and geochemically distinct locations. We further developed a novel approach for isolating protein-synthesizing cells identified using BONCAT via fluorescence-activated cell sorting (FACS). Subsequent 16S rRNA gene-based identification of individual AOM-consortia provided detailed aggregate-specific information into specific archaeal–bacterial partnerships. This approach revealed previously unrecognized metabolically active associations between ANME and new bacterial groups outside the deltaproteobacteria.

Results and Discussion

Establishment of HPG Incubation Experiments with Methane Seep Sediment. Samples were obtained from a methane seep from Hydrate Ridge, Oregon, (sample #3730), and a seep site in the Santa Monica Basin, California, (samples #7135, #7136-37, and #7142). Anoxic sediment microcosms were set up in the presence or absence of HPG (5 μM or 50 μM) and over-pressurized (2 bars) with either N_2 or methane followed by incubation in the dark at 4 °C for 114 d (#3730), 171 d (#7135), 31 d (#7136-37), and 25 d (#7142). These long incubation times were necessary due to the slow growth of ANME–SRB consortia (3–7 mo; e.g., refs. 41–43), which is attributed to the very low free energy yield of sulfate-coupled AOM (42, 44). Subsampling for molecular and geochemical analyses as well as exchange of gaseous headspace and seawater were conducted at regular intervals. Details on incubation setup and sampling is provided in Dataset S1.

HPG Amendment Had No Detectable Effect on Microbial Community Composition or Activity. Adding a compound to an environmental sample always bears the risk of altering the structure or function of the microbial community. Three independent lines of evidence suggest that, at the concentrations used in this study (≤50 μM), the methionine analog HPG did not affect the geochemical activity or community structure of microbes within methane seep sediment for up to 171 d of incubation. First, HPG addition had no effect on sulfide production, a reliable proxy for sulfate-dependent AOM activity (45) in time course experiments (up to 6 mo). In contrast, the removal of methane led to a notable and expected decrease (Fig. S1*A*) in sulfide production as previously reported (45). Second, seep sediment from Santa Monica Basin (sediment #7142) incubated with and without HPG over a period of 25 d showed equivalent rates of AOM, as measured by ^{13}C dissolved inorganic carbon (DIC) production following $^{13}CH_4$ amendment (Fig. S1*B*). Third, Illumina tag sequencing (iTAG) of the 16S rRNA V4 region of archaea and bacteria revealed that HPG additions had no statistically significant effect on sediment #3730 and #7135 community compositions (Figs. S2–S4). More specifically, control incubations of #3730 are indistinguishable from samples containing 50 μM HPG after 114 d of incubation (effect of HPG, $P = 0.20$), with an average Bray Curtis similarity of the communities of 94.4% between all samples (Figs. S2 and S3). Sequences related to ANME-2c archaea make up a slightly higher proportion in HPG-containing samples compared with incubations without HPG; however, this observation was not statistically supported (Figs. S3 and S5). Similarly, for #7135, no differences in the composition of the microbial community in general or ANME- and SRB-related lineages in particular between samples incubated in the presence (5 μM or 50 μM) or absence of HPG were observed (Figs. S2, S4, and S5). After 41 d, communities in incubations with or without HPG were, on average, 92.1% similar (Bray Curtis; effect of HPG, $P = 0.56$). This similarity decreased to 87.9–89.3% after an additional 130 d of incubation, but without a detectable effect from HPG ($P = 0.25$; Fig. S4*A*). The absence of methane in the headspace, however, did result in a statistically significant change in the microbial community ($P = 0.042$; Fig. S2*B*).

These independent activity and community composition analyses all indicate that the addition of the bioorthogonal amino acid HPG at concentrations up to 50 μM did not result in any detectable changes in the seep microbial diversity or activity up to 171 d.

Fluorescence Detection of Translationally Active Cells. To fluorescently label microbes undergoing active protein synthesis during the incubation, a recently established BONCAT protocol based on the Cu(I)-catalyzed conjugation of HPG with an azide dye (9, 14, 46) was used. In initial tests, no difference in fluorescence intensity or signal-to-noise ratio was observed between ethanol-fixed, paraformaldehyde-fixed, or nonfixed AOM consortia. All further experiments were thus performed on ethanol-fixed biomass, unless stated otherwise. Although several factors prohibit the absolute quantification of new proteins from fluorescence data (discussed in *SI Text*), semiquantitative comparisons between different cells of the same taxonomic group may offer information on the functional (translational) activity of uncultured cells in the environment. Throughout the text, we refer to DAPI-stained cell clusters that bound an ANME-specific (CARD) FISH probe as "microbial (AOM) consortia." When cells within a DAPI-stained cluster could not be unambiguously identified, we use the term "microbial aggregate" instead.

BONCAT as a Novel Approach to Study Anabolic Activity of AOM Consortia. To establish whether BONCAT can be used as a proxy for methane-dependent translational activity of AOM consortia, we used sample #7136-37, representing the 9- to 15-cm depth horizon immediately underlying sediment horizon #7135 (6–9 cm). After preincubation of the sediment in the absence of methane for 124 d, microcosm experiments were established with 50 μM HPG in the presence or absence of methane. After 31 d of incubation, microbial aggregates were extracted and analyzed by microscopy (n = 1,554). Under methane-replete conditions, 24.9% of all microbial aggregates were BONCAT-stained, whereas only 2.3% exhibited detectable translational activity when methane was absent from the headspace (Fig. 2). This initial test demonstrated that BONCAT can be used to study the methane-dependent anabolic activity of AOM consortia.

Sensitivity of BONCAT. In all incubations, the relative abundance of translationally active DAPI-stained microbial aggregates increased with time, with 65.8% and 48.5% of aggregates in #3730 and #7135 showing a positive BONCAT signal at the end of incubation (114 d and 171 d, respectively). It is interesting to note that, already after 7 d of incubation, 5.6% of the microbial aggregates in sediment #7135 were labeled by BONCAT (Fig. 2). Assuming that the AOM consortia studied here have growth rates comparable to those previously reported [2–7 mo (41, 42, 43)], we estimate that BONCAT is able to detect the activities of cells within ANME–SRB consortia after 3.3–7.7% of their doubling time. Considering the differences in the physiology of the organisms as well as the lower fluorescence signal-to-noise ratios observed in environmental systems, this estimate is consistent with our finding of a BONCAT detection limit of <2% of generation time for slow-growing *Escherichia coli* (9).

At this time, it is unclear why up to half of the DAPI-stained consortia were not BONCAT-stained during the AOM incubation experiments. This may have been the result of storing these deep-sea samples in the laboratory, variable amino acid uptake, or low levels of protein synthesis that are below detection with

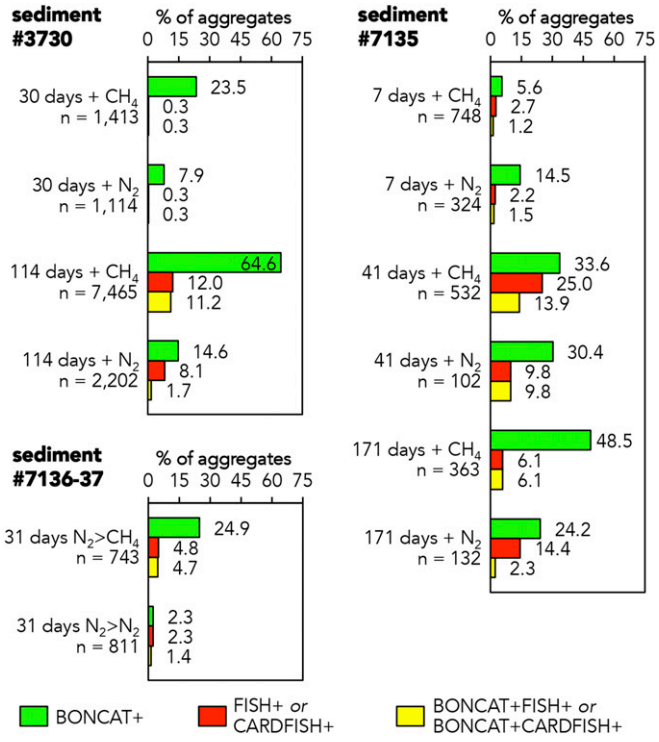

Fig. 2. Temporal dynamics of translational activities of microbial consortia as revealed by BONCAT-FISH. Three geographically distinct sediment samples, #3730, #7135, and #7136-37, were incubated in the presence of methane or N_2 for 114 d, 171 d, and 31 d, respectively; 2.3–30.4% of aggregates were translationally active in absence of methane, suggesting either the use of storage compounds, the presence of an endogenous methane source, or a potential physiological flexibility of these microbial partnerships. Green bars show the relative abundance of aggregates detectable via BONCAT. Red bars indicate the detection rate of DAPI-stained aggregates by FISH and CARD-FISH. Yellow bars give the relative abundance of aggregates that were both BONCAT-positive and FISH- or CARD-FISH-stained; n, number of microbial aggregates analyzed per experiment. For a list of probes and detailed results, see Dataset S2.

BONCAT. The combined application of BONCAT and rRNA-targeted FISH demonstrated that all ANME lineages present in our samples are able to incorporate HPG into their biomass (discussed in *Multiple Cooccurring ANME Subgroups Were Active Under Identical Incubation Conditions*). This suggests that an inability to take up HPG into cells is likely not a problem in our AOM microcosms. This idea is further supported by the observation that AHA and HPG are taken up and incorporated by a range of bacterial and archaeal cultures, including methanogens and sulfate reducers (9, 46).

BONCAT-FISH as a Tool for Microbial in Situ Activity Studies. Although the quantitative isotopic analysis provided by SIMS and nanoSIMS is currently unparalleled by other single cell techniques, the specialized instrumentation and cost along with comparatively lower sample throughput have restricted its widespread application in the field (10–100 consortia per study; e.g., refs. 7, 27, 35, and 36). Many fundamental questions in microbial ecology regarding the activity and metabolic potential of environmental microbes in situ, however, can be addressed with lower-precision methods.

To demonstrate the utility of BONCAT as a comparatively high-throughput method for tracking microbial biosynthetic activity, we used epifluorescence microscopy combined with FISH-BONCAT to investigate the translational activities of 14,884 individual microbial aggregates in the presence or absence of methane in microcosms mimicking in situ conditions. In total, 12,652 aggregates from four #3730 microcosms incubated for 30 d and 114 d were analyzed. In addition, the activities of 2,232 aggregates from six incubations of sediment #7135 after 7 d, 41 d, and 171 d of incubation were determined. To assess whether the activity of individual consortia is influenced by the phylogenetic affiliation of their partners, we combined BONCAT with rRNA-targeted FISH (Fig. 1*B*). Following our recently established protocol (9, 46), we used 11 different 16S and 23S rRNA-targeted oligonucleotide probes labeled with either a fluorescence dye or horseradish peroxidase (for catalyzed reporter deposition FISH, CARD-FISH) to target the different ANME populations and their associated bacteria present in our samples. These were applied in 11 different combinations (see *SI Text* and Datasets S2 and S3 for details) to study the activity of AOM consortia in the presence or absence of methane. In total, we visualized the translational activities of 1,346 taxonomically identified AOM consortia (representative images in Fig. 3; results in Fig. 2, Table 1, and Dataset S2).

BONCAT-FISH Reveals the Cooccurrence of Diverse and Active AOM Consortia. Domain-specific FISH probes (Arch915 and EUB338mix) hybridized 37.6% (114 d) and 51.8% (41 d) of microbial aggregates in methane-containing incubations of sediments #3730 and #7135, respectively. In contrast, the combined application of five fluorescently labeled oligonucleotide probes specific for the main ANME subpopulations present in our samples (ANME-1, -2a, -2b, and -2c) yielded positive results for only 5.4% (#3730, 114 d) and 5.8% (#7135, 41 d) of microbial aggregates in methane-containing samples. Two other groups of ANME archaea, nitrate-dependent ANME-2d (47) as well as ANME-3, were absent from our methane seep 16S rRNA iTAG datasets and thus were not probed by FISH. Compared with FISH, CARD-FISH yielded slightly lower detection rates for probe Arch915, specific for domain *Archaea* (55.7% in FISH vs. 53.2% for CARD-FISH for #3730, 114 d of incubation). Similar results were obtained for the combined application of ANME-specific probes, which, together, hybridized 4.2% of microbial aggregates (5.4% with FISH; Fig. 2 and Table 1). Comparable hybridization efficiencies were found for samples that had been incubated in the absence of HPG. Independent CARD-FISH experiments (Table 1 and *SI Text*) corroborated these findings.

The stark discrepancy between domain- and subpopulation-specific probes might be explained by a combination of factors. First, several available probes specific for different ANME clades are predicted to have low accessibilities to their rRNA target sites (48) and thus may exhibit low fluorescence signal-to-noise ratios. In addition, although most published ANME probes are predicted to comprehensively and specifically detect the diversity of sequences in rRNA databases, we do not know how well these probes cover the full diversity of ANME in the environment. For one subpopulation, ANME-2b, which was represented by 18–20% of all ANME-related tag sequences in our sediments (Fig. S5), we tried to overcome this problem by designing a new probe, ANME-2b-729. When tested in silico, this probe binds to 93% of all ANME-2b 16S rRNA sequences and has at least two mismatches to all non-ANME-2b-related rRNA sequences in public and in-house databases. We successfully applied this new probe to our sediment samples (Fig. 3 *D* and *E*), and the results are described in Table 1 and Dataset S2. Alternatively, it is possible that a fraction of DAPI-stained aggregates contained archaea unaffiliated to ANME. Similar to most other marine sediments (38), seep sediment #7135 from Santa Monica Basin hosts a variety of archaea unrelated to ANME (9–17% of all iTAG sequences in our dataset). The archaeal population in Hydrate Ridge sediment #3730, in contrast, is dominated by ANME (93.2–97.7% of all archaeal sequences). Therefore, it is unlikely that archaea unrelated to ANME constituted a substantial number of microbial consortia in #3730. Furthermore, to our knowledge, no other sediment-dwelling archaea have previously

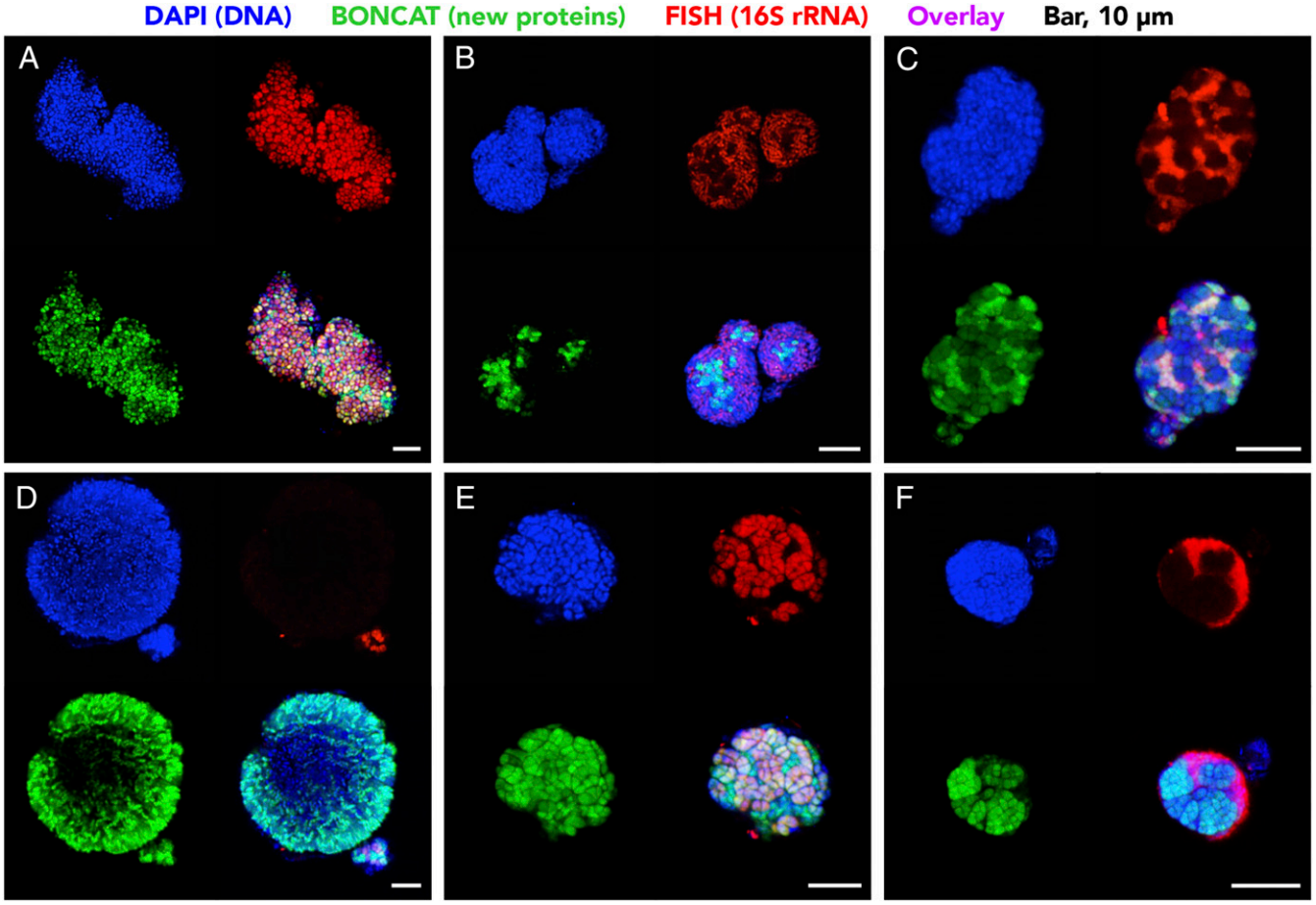

Fig. 3. Single-cell–resolved visualization of the wide range in translational activity observed for morphologically and taxonomically distinct methane-oxidizing consortia in sediment #3730. Protein synthesis-active cells were identified via BONCAT (green). The 16S rRNA-targeted oligonucleotide FISH probes, specific for the domain *Archaea* (*A* and *B*), most delta-proteobacteria (*C* and *F*), and ANME-2b (*D* and *E*), were used to taxonomically identify the two microbial partners (red). DAPI staining of DNA is shown in blue. An overlay of the three fluorescence channels and a 10-μm scale bar are shown at lower right in each panel. BONCAT-negative cells were either translationally inactive or have not taken up or incorporated HPG into new proteins.

been reported to occur in multicellular associations with bacteria. Additional discussions on FISH using ANME-specific probes can be found in the *SI Text*.

Of all consortia detectable with an ANME-specific FISH probe, 91.4% (sample #3730) and 81.8% (sample #7135) were also BONCAT-positive. In contrast, only 81.4% (#3730) and 58.3% (#7135) of all positively hybridized microbial aggregates (using either domain- or ANME-specific FISH probes) could be detected via BONCAT (Fig. 2 and Dataset S2). This result lends support to the view that rRNA-targeted FISH is not always a reliable proxy for cellular activity. Notably, there was no statistically supported relationship between BONCAT and FISH signal intensities of individual cells within AOM consortia ($n = 5$ consortia, each composed of 50–200 cells).

Multiple Cooccurring ANME Subgroups Were Active Under Identical Incubation Conditions. Methane seeps commonly harbor a wide range of taxonomically distinct ANME clades (e.g., refs. 26, 38, 49, and 50). The activity patterns and niche differentiation of these apparently functionally redundant groups are, however, not understood. So far, temperature (32), methane partial pressure (32), concentration of sulfate (33, 34) and sulfide (34), and nitrogen availability (35, 36) have directly or indirectly been shown to drive the abundance and activity of different ANME lineages. Using BONCAT, we were able to demonstrate that representatives of all major ANME subpopulations (ANME-1 and ANME-2a, -2b, and -2c) cooccurring in a sediment incubation were biosynthetically active under controlled AOM incubation conditions in the laboratory (Table 1). This result raises questions about the ecology underlying this apparent functional redundancy and factors influencing niche specialization. A promising approach for future studies of the functional capacities and niche adaptations of different ANME lineages will be to use isotopically labeled substrates in combination with BONCAT-based activity screening in targeted physiological experiments (9).

Table 1. Comparison of 16S rRNA gene-based affiliations of active ANME in sediment #3730 after 114 d of incubation in the presence of methane

No. of aggregates	FISH	CARDFISH	FACS
DAPI	2,946	1,130	
BONCAT+	1,922	678	34
(CARD) FISH+	167	48	
BONCAT+ and (CARD) FISH+	163	42	
% ANME-1	1	79	29
% ANME-2a	34	0	3
% ANME-2b	27	14	21
% ANME-2c	38	7	47

Activity of ANME–SRB Consortia in the Absence of methane. To date, members of ANME archaea have only been shown to conserve energy through methane oxidation. Some studies, however, have suggested that select ANME populations might be capable of methanogenesis (34, 51–55). Anabolic activity of individual ANME–SRB consortia in the absence of methane has not, however, been directly demonstrated. In our BONCAT-FISH studies, we found that, after 30 d of incubation without the addition of methane, 7.9% of DAPI-stained microbial aggregates from sediment #3730 were BONCAT-stained, and, after 114 d, this proportion nearly doubled to 14.6% [~50–95% of doubling time (41–43)]. A similar trend was observed for sample #7135 (14.5%, 30.4%, and 24.2% BONCAT-positive aggregates after 7 d, 41 d, and 171 d). This observation was in stark contrast to our #7136-37 incubations in the absence of methane, in which only a very small percentage (2.3%) of microbial aggregates were fluorescently labeled. Although #3730 and #7135 consortia were clearly BONCAT-stained, their fluorescence intensity was roughly 10-fold lower ($n = 20$) than consortia incubated in the presence of methane. Consistent with samples incubated in the presence of methane, the relative proportion of BONCAT-stained aggregates that could be attributed to a specific ANME population via (CARD) FISH was also very low in the absence of methane (0.3–9.8%; Fig. 2).

An explanation for activity of AOM consortia in the absence of methane headspace could be that some consortia may have the potential to consume previously accumulated energy storage compounds. This hypothesis is supported by the observation that some representatives of ANME-2b but not ANME-2c cells feature polyphosphate granules. Similarly, some ANME-associated SRB might harbor carbon storage compounds (56). Our results suggest that more AOM consortia than previously thought are able to build up substantial amounts of energy storage during times of substrate repletion. This is surprising, given the very low energy yield of the AOM reaction ($\Delta G^0 = -16$ kJ·mol^{-1} at standard conditions) (57). Our finding, however, is consistent with the observation that some AOM consortia are able to invest substantial amounts of metabolic energy in N_2 fixation (35, 58), one of the most energy-intensive reactions known (16 ATP per N_2).

The observation of an increase in active consortia in sediment #3730 over long periods of time (from 7.9% after 30 d to 14.7% after 114 d; Fig. 2) is, however, inconsistent with the predicted progressive depletion of storage compounds. Another possible explanation for results from #3730 could be attributed to an internal methane cycle, in which methanogens produced methane, which was then reoxidized by AOM consortia. Alternatively, members of ANME–SRB consortia might themselves engage in the production of methane rather than in sulfate-coupled AOM, as previously suggested (51–55). Recent experiments on the methanogenic potential of ANME-1 and ANME-2 enrichment cultures, however, have not supported this idea (59). A minor amount of methane was detected in our N_2-containing #3730 and #7136-37 microcosms; however, these levels were similar to concentrations measured as a trace contaminant in the N_2 tank (~1–10 ppm methane). The reported methane partial pressure capable of supporting AOM by methane seep consortia is 1 bar (i.e., 1.4 mM in solution) (32, 45), five orders of magnitude higher than concentrations in our incubations. Another intriguing possibility to explain the activity of BONCAT-stained ANME–SRB consortia in the absence of methane is that we might not yet recognize the full extent of physiological capabilities of ANME–SRB consortia and that they might be involved in energy conservation pathways unrelated to the oxidation or generation of methane. A first step toward formulating hypotheses about potential energy-yielding substrates is to identify specific archaeal–bacterial partnerships that might differ in their substrate range for targeted genomics.

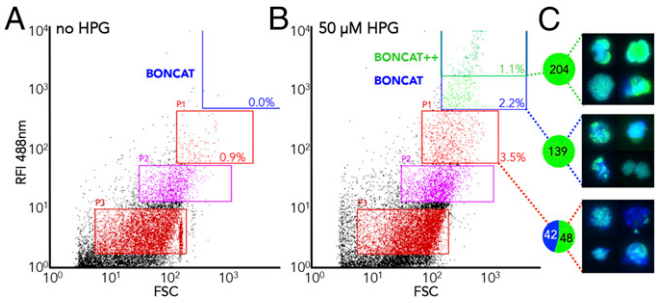

Fig. 4. Flow cytometric analysis of unfixed microbial cells and consortia extracted from sediment #3730 after incubation with (*A*) or without (*B*) HPG. (*C*) Microbial consortia detected by fluorescence microscopy after sorting of 200 events per gate. Only BONCAT and BONCAT++ gates were used for activity-based sorting. Microscopic images of representative tube-sorted consortia are on the right. Note that the relative fluorescence intensity differs between gates (for gate P1 events, exposure time had to be increased 10-fold compared with gate BONCAT to yield visually detectable BONCAT-fluorescence). RFI 488 nm is relative fluorescence intensity at an excitation of 488 nm; BONCAT++, BONCAT, P1, P2, and P3 are gates using for counting and sorting; gate P3 did only contain individual cells as well as sediment and Percoll particles. Percent values indicate the relative abundance of events within each gate.

Identification of Microbial Partners Within Activity-Sorted Consortia. With a few notable exceptions (10, 11, 39, 60–62), single-cell genome sequencing efforts so far have been "target-blind"; they did not select for a specific taxon of interest or focus on metabolically active cells that could be considered key species for ecosystem functioning. The power of these techniques to investigate microbial partnerships involved in AOM was recently demonstrated by the separation of FISH-identified ANME consortia from methane seep sediments via immunomagnetic capture [magneto-FISH (39, 63)] and fluorescent-activated cell sorting [FISH-FACS (61, 64)]. Using sorting approaches, associations between ANME and bacteria not known to be capable of sulfate reduction, including members of the alpha-, beta-, gamma- and epsilon-proteobacteria as well as *Planctomyces*, have been revealed (39). In addition, the potential of targeted sorting approaches for uncovering rare populations has been demonstrated by the successful enrichment of an ANME-2d population from ~2% to ~94% (61).

To demonstrate the potential of BONCAT to separate the functionally active fraction of a microbial community from complex samples, we sorted individual, translationally active consortia from sediments #3730 and #7142 by FACS. We refer to this activity-based cell-sorting approach as BONCAT-FACS (Fig. 1*C*). To test the specificity of the chosen gates, 200 events per gate were sorted into individual tubes and analyzed using fluorescence microscopy. For the BONCAT++ gate, which was used for all downstream analyses, 204 DAPI-stained microbial aggregates were identified, all of which were BONCAT-stained (Fig. 4). The slightly higher number of consortia (204 vs. the expected 200) may be due to cosorting of physically attached aggregates or the partial disaggregation of some aggregates after sorting.

Consortia sorted into individual wells of microtiter plates were lysed and their genomes amplified via multiple displacement amplification (MDA) following established protocols (65). For ethanol-fixed biomass from sediment #3730, 76 out of 168 sorted events resulted in an MDA product. This efficiency (45%) is comparable with that of a recent study that reported a success rate of 50% when DNA from cells stored in 70% ethanol was used as PCR template (66). By avoiding any cell fixation before sorting of individual consortia (Fig. 4), the efficiency of MDA reactions improved to 93% (78 out of 84 sorted events) for the same sample. Together, these results suggest that BONCAT and click

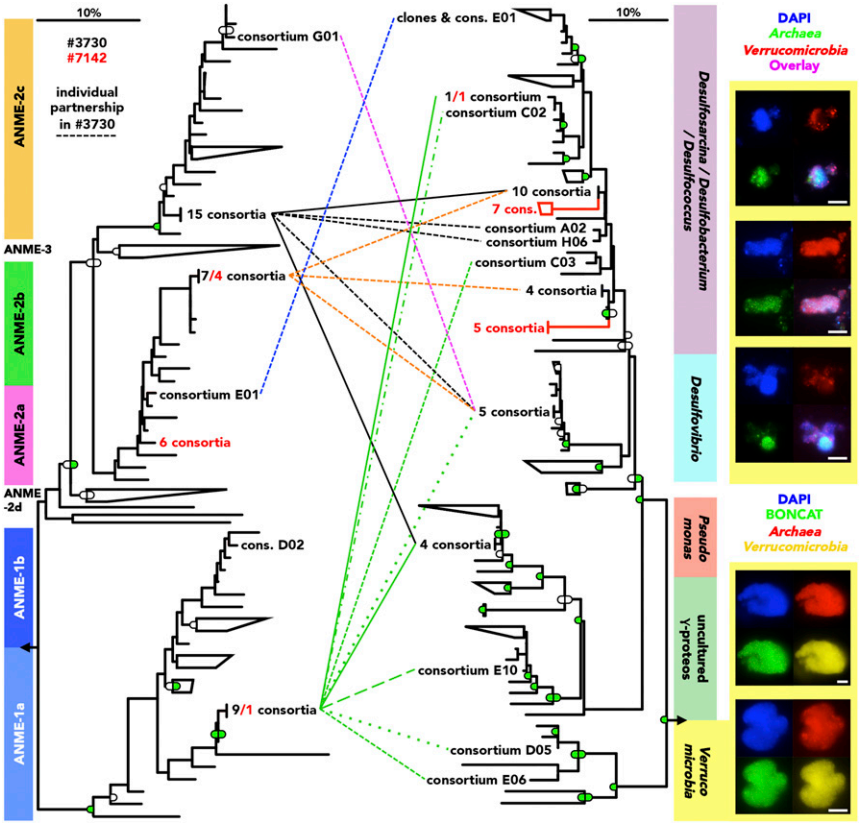

Fig. 5. Identification of microbial partners within AOM consortia after activity-based sorting. Taxonomic affiliation of the archaeal (left tree) and bacterial (right tree) partners within 45 individually sorted, translationally active consortia from sediments #3730 (black) after 114 d and #7142 (red) after 25 d of incubation with HPG. The potential to discover yet unrecognized microbial interactions with this approach is evidenced by our finding of two consortia containing *Verrucomicrobia*-derived sequences. Using FISH, we independently confirmed the presence and activity of microbial consortia composed of *Archaea* and *Verrucomicrobia* in several sediment and carbonate samples. Trees represent maximum likelihood reconstructions onto which bootstrap values are projected. Green and white colored boxes on trees show support ≥90% and ≥70%, respectively. Values <70% are not given. Boxes on left and right trees indicate maximum parsimony (100×) and neighbor joining (1,000×) values, respectively. Tag sequences were added after tree construction without changing overall tree topology. Solid and dashed lines indicate individual archaeal–bacterial partnerships. Scale bars equal 10% estimated sequence divergence. Detailed trees and additional FISH images are shown in Figs. S6 and S7.

chemistry-mediated dye labeling have no detrimental effect on DNA quality. Fixation of biomass was avoided for sediment #7142.

Diluted DNA from MDA reactions was used as the template in PCR amplifications targeting the V4 region of archaeal and bacterial 16S rRNA genes (67, 68). Amplicons from PCR reactions that yielded a single band during gel electrophoresis examination were barcoded, sequenced, and phylogenetically analyzed (Fig. 5 and Fig. S6). The majority of reactions contained both ANME- and SRB-related sequences in high numbers. In several reactions, however, only sequences from either the ANME or the SRB partner were obtained (sequences from the other cell type were <0.1%). Given the observed specificity for active microbial aggregates of our sorting approach (Fig. 4*B*), preferential amplification of a single sequence type for this subset may be indicative of bias during cell lysis and/or the MDA reaction, a problem well discussed in the literature (66, 69, 70). Reactions that only recovered SRB sequences ($n = 5$) were not considered further in our analysis. For each of the remaining 45 consortia, a single ANME operational taxonomic unit (OTU; defined here as a unique sequence) represented 93–100% of all ANME-associated sequences. Similarly, in each individual consortium from sediment #3730, a single OTU always contributed 94–100% of all SRB-related sequences. Despite the relatively low number of consortia analyzed ($n = 34$), representatives of all ANME clades found in #3730 samples (according to 16S rRNA iTAG data) were retrieved from a single incubation, corroborating the findings of phylogenetic diversity from our BONCAT-FISH studies (findings are summarized in Table 1). Consistent with previous reports (26, 36, 39, 49, 71), ANME-1 and ANME-2 were predominantly associated with putative sulfate reducers within the delta-proteobacterial lineages *Desulfobacterium*, *Desulfobulbus*, *Desulfococcus*, and *Desulfosarcina* (Fig. 5 and Fig. S6). Analysis of single consortia further revealed that individual ANME subpopulations (single OTU) are often associated with different bacterial partners, and vice versa. For example, the seven observed #3730 ANME-2b consortia (identical in their V4 region) have partners within three different bacterial families. Similarly, three consortia (A03Uf, C08Uf, and H01Uf) from sediment #7142 each harbored two SRB OTUs (94.9–98.8% identical in sequence).

In addition to sequences from SRB, five consortia from sediment #3730 also yielded low proportions of sequences from bacteria related to *Pseudomonas* or other gamma-proteobacteria (Fig. 5 and Fig. S6). These sequences were taxonomically different from commonly observed laboratory contaminants and were distinct from sequences detected in overamplified negative controls or control mock communities. This result, together with (*i*) the finding of highly similar gamma-proteobacterial sequences in a magneto-FISH study of AOM consortia (39), (*ii*) our demonstration that translationally active gamma-proteobacteria and archaea form consortia in sediment #3730 (Dataset S2), and (*iii*) the observation that individual ANME OTUs in different consortia were associated with diverse bacterial groups, lend strong support to the idea that AOM partnerships are dynamic, both in terms of partner affiliation and possibly their ecophysiology (39).

Discovery of a New Interdomain Partnership. The rRNA gene sequences obtained from an ANME-1a consortium (#E06) from #3730 did not contain sequences related to known sulfate reducers, but instead recovered sequences associated with *Verrucomicrobia*. Sequences retrieved from a second consortium (#D05) also contained the same ANME-1a OTU, in addition to both *Desulfobulbaceae* sequences and another *Verrucomicrobia*-affiliated OTU (sequence 80% identical to the E06 OTU). Both *Verrucomicrobia*-affiliated sequences had ≤81% identity to rRNA genes from previously described species (Fig. 5 and Fig. S6).

To complement our sequence-based observations, we used FISH to screen 27 samples from nine methane seep sediment cores obtained from a variety of geographic locations as well as two carbonates retrieved from a methane vent site for the

association of *Verrucomicrobia* with AOM consortia. We used two 16S rRNA-targeted probes specific for the phylum *Verrucomicrobia* (EUB338-III and Ver47) (72–74), in combination with the general archaeal probe Arch915, to screen archaeal aggregates from these samples. In four sediments (#3730 incubated for 30 d and 114 d in the presence of HPG and methane; sediments #5119, #5202, and #7142) as well as both carbonate samples (#2450 and #3439), verrucomicrobial cells were associated with 10–20% of AOM consortia (Dataset S3 and Fig. S7). Although the vast majority (~98%) of these aggregates contained only low numbers of *Verrucomicrobia* (<20 per aggregate), a small number ($n = 14$) of aggregates exhibited very high ratios of verrucomicrobial to archaeal cells (Fig. 5, Fig. S7, and Dataset S3).

Despite the near-ubiquitous distribution of *Verrucomicrobia* in marine sediments (75), including all 23 methane seeps recently surveyed via 16S iTAG sequencing (38), archaeal–verrucomicrobial associations have not been described previously. Because of the loss of structural information during DNA extraction and the typically low abundance of consortia consisting of ANME and nontraditional partner bacteria (refs. 39 and 40 and this study), metagenomic sequencing has so far failed to provide metabolic predictions on the whole diversity of these microbial associations. Our results reinforce the imperative to combine genomic sequencing with spatially resolved approaches, such as microscopy and cell sorting (e.g., refs. 10, 69, and 76), to gain access to the genetic potential of these important associations.

At this time, we can only speculate about the biological necessities driving the physical association of *Verrucomicrobia* with ANME. The low relative abundance of *Verrucomicrobia* associated with AOM consortia, however, suggests that these cells might be heterotrophs, consuming organic exudates or exopolymers of the archaeal cells. A similar cross-feeding relationship has previously been hypothesized for anammox bacteria cooccurring with ANME-2d archaea (47). Genomic sequencing of individual ANME–*Verrucomicrobia* aggregates sorted via BONCAT-FACS combined with additional microcosm experiments may assist with expanding our understanding of the nature of these ANME–verrucomicrobial interactions.

Conclusion and Outlook

The possibility of detecting anabolic activity of taxonomically identified cells using fluorescence staining offers a valuable complement to existing fluorescence microscopy methods for microbial ecology. BONCAT-FISH allows the activity screening of thousands of cells within a few hours, rather than a few dozen per day as achieved by isotope labeling techniques. Both bioorthogonal (this study) and nondestructive isotope labeling (10, 60) approaches further allow the sorting of individual cells and aggregates from complex samples, although sorting throughput for BONCAT-FACS is much higher. Sorted cells can be subjected to whole-genome amplification (WGA) and sequencing, thus allowing direct access to the genetic potential of cells functionally important under defined conditions. In contrast to isotope labeling approaches, which test whether cells are able to assimilate a specific substrate of interest (1, 5, 6, 77), BONCAT is an untargeted marker of translational activity. Hence, BONCAT cannot directly provide information about specific substrate metabolism, as is possible with isotope probing. However, the possibility of combining BONCAT-incubations with the addition of any other compound allows for in situ metabolic screening and comparative analysis of organisms stimulated by the compound (9). Thus, we anticipate that BONCAT-FISH will be particularly attractive if nonassimilatory pathways or substrates that are not (or only very expensively) available as stable isotope-labeled derivatives are to be studied. Growth-promoting substrates could, in the following, be used for the targeted cultivation of translationally responsive cells. In contrast to isotope labeling approaches, which require specialized instrumentation, BONCAT-FISH and BONCAT-FACS use standard configuration microscopes and flow cytometers that are more readily available to molecular biological laboratories.

Here, we established that HPG at concentrations up to 50 μM can be applied to marine methane seep sediments without detectable effects on the structure and function of the microbial community. We demonstrate that the subsequent detection of HPG-containing de novo synthesized proteins via click chemistry is a powerful approach to visualizing and identifying translationally active microbes in situ, separating them from complex samples via activity-based cell sorting, and studying microbial interactions. We demonstrate that representatives of all major subgroups of ANME are functionally active in Hydrate Ridge seep sediments. In addition, we show that, in two geographically distinct sediments, some consortia are active in the absence of methane. It remains to be tested whether these findings are entirely the result of the use of cellular storage materials or a physiological flexibility of these archaea that is yet unaccounted for. Furthermore, we provide the first evidence, to our knowledge, for the existence of previously unrecognized interactions of archaea and *Verrucomicrobia* in marine sediments. We anticipate that genomic characterizations of these as well as other diverse ANME–SRB consortia will soon provide hypotheses about potential growth-supporting substrates, and that BONCAT-FISH and BONCAT-FACS will play important roles in experimentally testing the ecophysiological properties of these globally relevant microbial partnerships.

Materials and Methods

Incubation of Methane Seep Sediment. Samples were obtained from three sediment cores taken off the coasts of California (Santa Monica Basin) and Oregon (Hydrate Ridge) and incubated in the presence of absence of HPG and methane for up to 6 mo. Samples for geochemical characterization, whole-community composition, and microscopic analyses were taken in regular intervals. Details on these experimental procedures are described in *SI Text*.

BONCAT. BONCAT was performed following our recently established protocol without modifications (46). Succinctly, fixed biomass (whole sediment or extracted consortia) was immobilized on Teflon-coated glass slides and dried at 46 °C. An increasing ethanol series [50%, 80%, and 96% ethanol in double-distilled water (ddH_2O)] was performed, and the slides were air-dried. Solutions were prepared as recently described (46), and the "click cocktail" was always freshly mixed. This solution contained 5 mM sodium ascorbate (Sigma-Aldrich), 5 mM amino-guanidine hydrochloride (Sigma-Aldrich), 500 μM Tris[(1-hydroxypropyl-1*H*-1,2,3-triazol-4-yl)methyl]amine (THPTA; Click Chemistry Tools), 100 μM $CuSO_4$ (Sigma-Aldrich), and 2 μM of azide-modified dye carboxyrhodamine 110 (CR-110; Click Chemistry Tools) or azide-modified 5(6)-carboxytetramethylrhodamine (TAMRA; Click Chemistry Tools) (used only in combination with CARD-FISH) in 0.2-μm-filtered 1× PBS, pH 7.4; 20 μL of this solution was applied on top of biomass, and the glass slides were incubated for 60 min at room temperature (RT) in a humid chamber. Afterward, slides were washed repeatedly in 1× PBS and an increasing ethanol series (50%, 80%, and 96%), before being air-dried. For details on this protocol, see Hatzenpichler and Orphan (46) and Hatzenpichler et al. (9). Nonfixed samples were processed following the same protocol with the difference that all ethanol washing steps were omitted.

FISH and CARD FISH. Following BONCAT, ethanol-washed samples were hybridized with oligonucleotide probes. For FISH experiments, double-labeled (78) or monolabeled probes with either Cy3 or Cy5 fluorescence dyes were used. FISH hybridizations were performed overnight (14–18 h) according to standard protocols (9, 79). The quality of all probe solutions (except ANME-2-932) was checked using other seep samples before they were applied to #3730 and #7135-37 sediments. All tested probe solutions yielded a large number of positive hybridizations to AOM consortia in these control samples. Each probe or probe set was hybridized in a technical duplicate or triplicate. No differences in fluorescence intensity or relative proportion of (CARD) FISH-positive consortia could be observed between replicate hybridizations.

CARD-FISH was performed as recently described (80). Three different cell wall digestion protocols were tested, but only one, a modified version of a recently published protocol (36), was found to be successful. Permeabilization was performed at RT as follows: incubation in 0.01 M HCl for 15 min; two washing steps in ddH_2O, 1 min each; incubation in 0.5% sodium dodecyl sulfate for 5 min; three washing steps in ddH_2O, 1 min each; incubation in 50% (vol/vol) ethanol in ddH_2O for 1 min. After air-drying, samples were hybridized for 14–18 h with horseradish peroxidase-conjugated oligonucleotides

(purchased from Biomers) before signal amplification using self-synthesized fluorescein-labeled tyramide was carried out.

Microscopy and Image Analysis. Samples were mounted with 1 mg·mL^{-1} 4,6-diamidino-2-phenylindole (DAPI; Sigma-Aldrich) in Citifluor AF-1 antifading solution (Electron Microscopy Sciences) and analyzed using either an Olympus BX51 epifluorescence microscope or a Zeiss LSM-510-Meta confocal laser-scanning microscope. Images were analyzed using the ImageJ software (NIH). In total, 12,652, 2,232, and 1,554 consortia were analyzed for sediments #3730, #7135, and #7136-37, respectively. The lower number of consortia analyzed for the latter samples is explained by the much lower concentration of AOM consortia in that sediment core. Each DAPI-stained microbial aggregate was manually inspected for BONCAT and FISH signals, and representative images were taken for each probe set. Consortia were always identified via DAPI, before switching to the other fluorescent channels to not preferentially select for BONCAT-positive or FISH-positive consortia. A detailed list of BONCAT-FISH counts can be found in Datasets S2 and S3. In every BONCAT-positive aggregate, either (*i*) (nearly) all cells within an aggregate were stained or, in rare cases, (*ii*) (nearly) all cells of one (but not the other) cell type (archaea or bacteria) were stained. Given the complex 3D structure of the aggregates, which sometimes grow many thousands of cells large (Fig. 3*A*), we cannot exclude that, in rare cases, individual cells (<5%) of a specific cell type were not stained (hence the term "nearly all").

After shipping and storage at 4 °C for 3 d, activity-sorted consortia were resuspended in 1 mL 1× PBS before being harvested by centrifugation (5 min at 16,100 × *g*; RT), resuspended in 1:1 1× PBS:ethanol, and immobilized on a glass slide. The slide was washed for 1 min in 50% ethanol (in ddH_2O), air-dried, DAPI-embedded, and microscopically analyzed. Consortia were counted following the same procedure as outlined above, and representative images were taken.

Activity-Based Cell Sorting. Initial tests were performed using pure cultures and mixtures of *E. coli* K-12, *Methyloprofundus sedimenti* WF-1 (81), and *Desulfovibrio alaskensis* G20 that had been incubated in the absence or presence (250 μM) of HPG for approximately one generation and stained using an azide-modified version of dye CR110 as recently described (9, 46). After successful tests, BONCAT-treated sediment-extracted consortia from samples #3730 and #7142 were analyzed. A BD Influx cell sorter was sterilized, and sheath fluid was prepared using 1× PBS, as recently described (65). After passing through a 70-μm nylon mesh filter, samples were sorted using a 200-μm nozzle at 0.21 bar. The sort mode was "1.0 drop single"; 2× 84 single events were deposited into wells E4–L15 of two 384-well plates, with rows D and L serving as negative control wells. BONCAT dye CR110 was excited using a 488-nm laser, and fluorescence was captured with a 531-nm/30-nm filter. Gates were defined using a forward scatter (FSC) vs. 531-nm emission plot, and events with a BONCAT signal brighter than >90% of aggregates in the negative control were captured (Fig. 4). For quantification of sorted consortia, 200 events identified within each gate were sorted into 1.5-mL tubes that contained 10 μL 1× PBS. Tubes were stored at 4 °C until further processing.

Sequence Access. Sequences have been deposited in the National Center for Biotechnology Information GenBank database under accession nos. KT945170–KT945234 and KU564217–KU564240 (16S rRNA iTAG sequences from activity-sorted consortia in #3730 and #7142, respectively) and Sequence Read Archive under accession no. SRP066109 (whole-community 16S rRNA iTAG sequences).

ACKNOWLEDGMENTS. We thank Alexis Pasulka and Kat Dawson for shipboard sample processing, Silvan Scheller and Kat Dawson for measurements of AOM rates and methane concentrations, Hang Yu for performing cline assays, Connor Skennerton for help during sampling of sediment incubations, David Case for discussions on tag sequence analyses, and Shawn McGlynn for discussions on storage compounds. David Case, Kat Dawson, and Elizabeth Wilbanks are acknowledged for critical comments on the manuscript. We thank The Biological Imaging Facility of California Institute of Technology for access to their confocal microscope. We thank the crew and pilots of R/V *Atlantis* Cruises AT-15-68 and AT-18-10 to Hydrate Ridge (supported by National Science Foundation Grant OCE-0825791) and the R/V *Western Flyer* Cruise to Santa Monica Basin run by the Monterey Bay Aquarium Research Institute. R.H. was supported by an Erwin Schrödinger Postdoctoral Fellowship from the Austrian Science Fund (FWF) (project no. J 3162-B20), and a postdoctoral fellowship from the Center for Dark Energy Biosphere Investigations (C-DEBI). Funding for this project was provided by Gordon and Betty Moore Foundation Grant GBMF3780 (to V.J.O.), Department of Energy (DOE) Grant DE-PS02-09ER09-25 (to V.J.O.), and a JGI Director Discretionary Project Award (to R.H. and V.J.O.). The work conducted by the DOE Joint Genome Institute, a DOE Office of Science User Facility, is supported under Contract DE-AC02-05CH11231. This is C-DEBI Contribution 330.

1. Neufeld JD, Wagner M, Murrell JC (2007) Who eats what, where and when? Isotope-labelling experiments are coming of age. *ISME J* 1(2):103–110.
2. Moran MA, et al. (2013) Sizing up metatranscriptomics. *ISME J* 7(2):237–243.
3. VerBerkmoes NC, Denef VJ, Hettich RL, Banfield JF (2009) Systems biology: Functional analysis of natural microbial consortia using community proteomics. *Nat Rev Microbiol* 7(3):196–205.
4. Orphan VJ (2009) Methods for unveiling cryptic microbial partnerships in nature. *Curr Opin Microbiol* 12(3):231–237.
5. Wagner M (2009) Single-cell ecophysiology of microbes as revealed by Raman microspectroscopy or secondary ion mass spectrometry imaging. *Annu Rev Microbiol* 63: 411–429.
6. Lee N, et al. (1999) Combination of fluorescent in situ hybridization and microautoradiography—A new tool for structure-function analyses in microbial ecology. *Appl Environ Microbiol* 65(3):1289–1297.
7. Orphan VJ, House CH, Hinrichs KU, McKeegan KD, DeLong EF (2001) Methane-consuming archaea revealed by directly coupled isotopic and phylogenetic analysis. *Science* 293(5529):484–487.
8. Huang WE, et al. (2007) Raman-FISH: Combining stable-isotope Raman spectroscopy and fluorescence in situ hybridization for the single cell analysis of identity and function. *Environ Microbiol* 9(8):1878–1889.
9. Hatzenpichler R, et al. (2014) *In situ* visualization of newly synthesized proteins in environmental microbes using amino acid tagging and click chemistry. *Environ Microbiol* 16(8):2568–2590.
10. Berry D, et al. (2015) Tracking heavy water (D_2O) incorporation for identifying and sorting active microbial cells. *Proc Natl Acad Sci USA* 112(2):E194–E203.
11. Kalyuzhnaya MG, Lidstrom ME, Chistoserdova L (2008) Real-time detection of actively metabolizing microbes by redox sensing as applied to methylotroph populations in Lake Washington. *ISME J* 2(7):696–706.
12. Konopka MC, et al. (2011) Respiration response imaging for real-time detection of microbial function at the single-cell level. *Appl Environ Microbiol* 77(1):67–72.
13. Smriga S, Samo TJ, Malfatti F, Villareal J, Azam F (2014) Individual cell DNA synthesis within natural marine bacterial assemblages as detected by 'click' chemistry. *Aquat Microb Ecol* 72(3):269–280.
14. Samo TJ, Smriga S, Malfatti F, Sherwood BP, Azam F (2014) Broad distribution and high proportion of protein synthesis active marine bacteria revealed by click chemistry at the single cell level. *Front Mar Sci Aquat Microbiol* 1:48.
15. Dieterich DC, et al. (2007) Labeling, detection and identification of newly synthesized proteomes with bioorthogonal non-canonical amino-acid tagging. *Nat Protoc* 2(3): 532–540.
16. Dieterich DC, Link AJ, Graumann J, Tirrell DA, Schuman EM (2006) Selective identification of newly synthesized proteins in mammalian cells using bioorthogonal noncanonical amino acid tagging (BONCAT). *Proc Natl Acad Sci USA* 103(25): 9482–9487.
17. Kiick KL, Saxon E, Tirrell DA, Bertozzi CR (2002) Incorporation of azides into recombinant proteins for chemoselective modification by the Staudinger ligation. *Proc Natl Acad Sci USA* 99(1):19–24.
18. Ngo JT, Tirrell DA (2011) Noncanonical amino acids in the interrogation of cellular protein synthesis. *Acc Chem Res* 44(9):677–685.
19. Bagert JD, et al. (2014) Quantitative, time-resolved proteomic analysis by combining bioorthogonal noncanonical amino acid tagging and pulsed stable isotope labeling by amino acids in cell culture. *Mol Cell Proteomics* 13(5):1352–1358.
20. Sinai L, Rosenberg A, Smith Y, Segev E, Ben-Yehuda S (2015) The molecular timeline of a reviving bacterial spore. *Mol Cell* 57(4):695–707.
21. Beatty KE, Tirrell DA (2008) Two-color labeling of temporally defined protein populations in mammalian cells. *Bioorg Med Chem Lett* 18(22):5995–5999.
22. Dieterich DC, et al. (2010) In situ visualization and dynamics of newly synthesized proteins in rat hippocampal neurons. *Nat Neurosci* 13(7):897–905.
23. Beatty KE, et al. (2006) Fluorescence visualization of newly synthesized proteins in mammalian cells. *Angew Chem Int Ed Engl* 45(44):7364–7367.
24. Beatty KE, Xie F, Wang Q, Tirrell DA (2005) Selective dye-labeling of newly synthesized proteins in bacterial cells. *J Am Chem Soc* 127(41):14150–14151.
25. Reeburgh WS (2007) Oceanic methane biogeochemistry. *Chem Rev* 107(2):486–513.
26. Boetius A, et al. (2000) A marine microbial consortium apparently mediating anaerobic oxidation of methane. *Nature* 407(6804):623–626.
27. McGlynn SE, Chadwick GL, Kempes CP, Orphan VJ (2015) Single cell activity reveals direct electron transfer in methanotrophic consortia. *Nature* 526(7574):531–535.
28. Wegener G, Krukenberg V, Riedel D, Tegetmeyer HE, Boetius A (2015) Intercellular wiring enables electron transfer between methanotrophic archaea and bacteria. *Nature* 526(7574):587–590.
29. Scheller S, Hang Y, Chadwick GL, McGlynn SE, Orphan VJ (2016) Artificial electron acceptors decouple archaeal methane oxidation from sulfate reduction. *Science* 351(6274):703–707.
30. Milucka J, et al. (2012) Zero-valent sulphur is a key intermediate in marine methane oxidation. *Nature* 491(7425):541–546.
31. Moran JJ, et al. (2008) Methyl sulfides as intermediates in the anaerobic oxidation of methane. *Environ Microbiol* 10(1):162–173.
32. Nauhaus K, Treude T, Boetius A, Krüger M (2005) Environmental regulation of the anaerobic oxidation of methane: A comparison of ANME-I and ANME-II communities. *Environ Microbiol* 7(1):98–106.

33. Yanagawa K, et al. (2011) Niche separation of methanotrophic archaea (ANME-1 and -2) in methane-seep sediments of the eastern Japan Sea offshore Joetsu. *Geomicrobiol J* 28(2): 118–129.
34. Timmers PH, Widjaja-Greefkes HC, Ramiro-Garcia J, Plugge CM, Stams AJ (2015) Growth and activity of ANME clades with different sulfate and sulfide concentrations in the presence of methane. *Front Microbiol* 6:988.
35. Dekas AE, Poretsky RS, Orphan VJ (2009) Deep-sea archaea fix and share nitrogen in methane-consuming microbial consortia. *Science* 326(5951):422–426.
36. Green-Saxena A, Dekas AE, Dalleska NF, Orphan VJ (2014) Nitrate-based niche differentiation by distinct sulfate-reducing bacteria involved in the anaerobic oxidation of methane. *ISME J* 8(1):150–163.
37. Knittel K, Lösekann T, Boetius A, Kort R, Amann R (2005) Diversity and distribution of methanotrophic archaea at cold seeps. *Appl Environ Microbiol* 71(1):467–479.
38. Ruff SE, et al. (2015) Global dispersion and local diversification of the methane seep microbiome. *Proc Natl Acad Sci USA* 112(13):4015–4020.
39. Pernthaler A, et al. (2008) Diverse syntrophic partnerships from deep-sea methane vents revealed by direct cell capture and metagenomics. *Proc Natl Acad Sci USA* 105(19):7052–7057.
40. Trembath-Reichert E, Case DH, Orphan VJ (2016) Characterization of microbial associations with methanotrophic archaea and sulfate-reducing bacteria through statistical comparison of nested Magneto-FISH enrichments. *PeerJ* 4:e1913.
41. Girguis PR, Orphan VJ, Hallam SJ, DeLong EF (2003) Growth and methane oxidation rates of anaerobic methanotrophic archaea in a continuous-flow bioreactor. *Appl Environ Microbiol* 69(9):5472–5482.
42. Nauhaus K, Albrecht M, Elvert M, Boetius A, Widdel F (2007) *In vitro* cell growth of marine archaeal–bacterial consortia during anaerobic oxidation of methane with sulfate. *Environ Microbiol* 9(1):187–196.
43. Orphan VJ, Turk KA, Green AM, House CH (2009) Patterns of ^{15}N assimilation and growth of methanotrophic ANME-2 archaea and sulfate-reducing bacteria within structured syntrophic consortia revealed by FISH-SIMS. *Environ Microbiol* 11(7):1777–1791.
44. Larowe DE, Dale AW, Regnier P (2008) A thermodynamic analysis of the anaerobic oxidation of methane in marine sediments. *Geobiology* 6(5):436–449.
45. Nauhaus K, Boetius A, Krüger M, Widdel F (2002) *In vitro* demonstration of anaerobic oxidation of methane coupled to sulphate reduction in sediment from a marine gas hydrate area. *Environ Microbiol* 4(5):296–305.
46. Hatzenpichler R, Orphan VJ (2015) Detection of protein-synthesizing microorganisms in the environment via bioorthogonal non-canonical amino acid tagging (BONCAT). *Single-Cell and Single-Molecule Methods*, Hydrocarbon and Lipid Microbiology Protocols, ed McGenity TJ (Springer, Berlin), Vol 7, pp 145–157.
47. Haroon MF, et al. (2013) Anaerobic oxidation of methane coupled to nitrate reduction in a novel archaeal lineage. *Nature* 500(7464):567–570.
48. Behrens S, et al. (2003) *In situ* accessibility of small-subunit rRNA of members of the domains *Bacteria, Archaea*, and *Eucarya* to Cy3-labeled oligonucleotide probes. *Appl Environ Microbiol* 69(3):1748–1758.
49. Orphan VJ, et al. (2001) Comparative analysis of methane-oxidizing archaea and sulfate-reducing bacteria in anoxic marine sediments. *Appl Environ Microbiol* 67(4): 1922–1934.
50. Orphan VJ, House CH, Hinrichs KU, McKeegan KD, DeLong EF (2002) Multiple archaeal groups mediate methane oxidation in anoxic cold seep sediments. *Proc Natl Acad Sci USA* 99(11):7663–7668.
51. Lloyd KG, Alperin MJ, Teske A (2011) Environmental evidence for net methane production and oxidation in putative ANaerobic MEthanotrophic (ANME) archaea. *Environ Microbiol* 13(9):2548–2564.
52. Orcutt B, Boetius A, Elvert M, Samarkin V, Joye SB (2005) Molecular biogeochemistry of sulfate reduction, methanogenesis and the anaerobic oxidation of methane at Gulf of Mexico cold seeps. *Geochim Cosmochim Acta* 69(17):4267–4281.
53. Treude T, et al. (2007) Consumption of methane and CO_2 by methanotrophic microbial mats from gas seeps of the anoxic Black Sea. *Appl Environ Microbiol* 73(7): 2271–2283.
54. Bertram S, et al. (2013) Methanogenic capabilities of ANME-archaea deduced from ^{13}C-labelling approaches. *Environ Microbiol* 15(8):2384–2393.
55. House CH, et al. (2009) Extensive carbon isotopic heterogeneity among methane seep microbiota. *Environ Microbiol* 11(9):2207–2215.
56. Heller C, Hoppert M, Reitner A (2008) Immunological localization of coenzyme M reductase in anaerobic methane-oxidizing Archaea of ANME 1 and ANME 2. *Geomicrobiol J* 25(3-4):149–156.
57. Knittel K, Boetius A (2009) Anaerobic oxidation of methane: Progress with an unknown process. *Annu Rev Microbiol* 63:311–334.
58. Dekas AE, Connon SA, Chadwick GL, Trembath-Reichert E, Orphan VJ (2016) Activity and interactions of methane seep microorganisms assessed by parallel transcription and FISH-NanoSIMS analyses. *ISME J* 10(3):678–692.
59. Wegener G, Krukenberg V, Ruff SE, Kellermann MY, Knittel K (2016) Metabolic capabilities of microorganisms involved in and associated with the anaerobic oxidation of methane. *Front Microbiol* 7:46.
60. Huang WE, Ward AD, Whiteley AS (2009) Raman tweezers sorting of single microbial cells. *Environ Microbiol Rep* 1(1):44–49.
61. Yilmaz S, Haroon MF, Rabkin BA, Tyson GW, Hugenholtz P (2010) Fixation-free fluorescence *in situ* hybridization for targeted enrichment of microbial populations. *ISME J* 4(10):1352–1356.
62. Kashtan N, et al. (2014) Single-cell genomics reveals hundreds of coexisting subpopulations in wild *Prochlorococcus*. *Science* 344(6182):416–420.
63. Trembath-Reichert E, Green-Saxena A, Orphan VJ (2013) Whole cell immunomagnetic enrichment of environmental microbial consortia using rRNA-targeted Magneto-FISH. *Methods Enzymol* 531:21–44.
64. Lösekann T, et al. (2007) Diversity and abundance of aerobic and anaerobic methane oxidizers at the Haakon Mosby Mud Volcano, Barents Sea. *Appl Environ Microbiol* 73(10):3348–3362.
65. Rinke C, et al. (2014) Obtaining genomes from uncultivated environmental microorganisms using FACS-based single-cell genomics. *Nat Protoc* 9(5):1038–1048.
66. Clingenpeel S, Schwientek P, Hugenholtz P, Woyke T (2014) Effects of sample treatments on genome recovery via single-cell genomics. *ISME J* 8(12):2546–2549.
67. Caporaso JG, et al. (2012) Ultra-high-throughput microbial community analysis on the Illumina HiSeq and MiSeq platforms. *ISME J* 6(8):1621–1624.
68. Caporaso JG, et al. (2011) Global patterns of 16S rRNA diversity at a depth of millions of sequences per sample. *Proc Natl Acad Sci USA* 108(Suppl 1):4516–4522.
69. Rinke C, et al. (2013) Insights into the phylogeny and coding potential of microbial dark matter. *Nature* 499(7459):431–437.
70. Clingenpeel S, Clum A, Schwientek P, Rinke C, Woyke T (2015) Reconstructing each cell's genome within complex microbial communities-dream or reality? *Front Microbiol* 5:771.
71. Kleindienst S, Ramette A, Amann R, Knittel K (2012) Distribution and in situ abundance of sulfate-reducing bacteria in diverse marine hydrocarbon seep sediments. *Environ Microbiol* 14(10):2689–2710.
72. Daims H, Brühl A, Amann R, Schleifer KH, Wagner M (1999) The domain-specific probe EUB338 is insufficient for the detection of all *Bacteria*: Development and evaluation of a more comprehensive probe set. *Syst Appl Microbiol* 22(3):434–444.
73. Arnds J, Knittel K, Buck U, Winkel M, Amann R (2010) Development of a 16S rRNA-targeted probe set for Verrucomicrobia and its application for fluorescence in situ hybridization in a humic lake. *Syst Appl Microbiol* 33(3):139–148.
74. Bergen B, Herlemann DP, Labrenz M, Jürgens K (2014) Distribution of the verrucomicrobial clade *Spartobacteria* along a salinity gradient in the Baltic Sea. *Environ Microbiol Rep* 6(6):625–630.
75. Freitas S, et al. (2012) Global distribution and diversity of marine *Verrucomicrobia*. *ISME J* 6(8):1499–1505.
76. Blainey PC (2013) The future is now: single-cell genomics of bacteria and archaea. *FEMS Microbiol Rev* 37(3):407–427.
77. Orphan VJ, House CH (2009) Geobiological investigations using secondary ion mass spectrometry: Microanalysis of extant and paleo-microbial processes. *Geobiology* 7(3): 360–372.
78. Stoecker K, Dorninger C, Daims H, Wagner M (2010) Double labeling of oligonucleotide probes for fluorescence in situ hybridization (DOPE-FISH) improves signal intensity and increases rRNA accessibility. *Appl Environ Microbiol* 76(3):922–926.
79. Daims H, Stoecker K, Wagner M (2005) Fluorescence *in situ* hybridization for the detection of prokaryotes. *Advanced Methods in Molecular Microbial Ecology*, eds Osborn AM, Smith CJ (Bios Garland, Abingdon), pp 213–239.
80. Hatzenpichler R, et al. (2008) A moderately thermophilic ammonia-oxidizing crenarchaeote from a hot spring. *Proc Natl Acad Sci USA* 105(6):2134–2139.
81. Tavormina PL, et al. (2015) *Methyloprofundus sedimenti* gen. nov., sp. nov., an obligate methanotroph from ocean sediment belonging to the 'deep sea-1' clade of marine methanotrophs. *Int J Syst Evol Microbiol* 65(Pt 1):251–259.
82. Cline JD (1969) Spectrophotometric determination of hydrogen sulfide in natural waters. *Limnol Oceanogr* 14(3):454–458.
83. Stahl DA, Amann R (1991) Development and application of nucleic acid probes. *Nucleic Acid Techniques in Bacterial Systematics*, eds Stackebrandt EG, Goodfellow M (John Wiley, New York), pp 205–248.
84. Amann RI, et al. (1990) Combination of 16S rRNA-targeted oligonucleotide probes with flow cytometry for analyzing mixed microbial populations. *Appl Environ Microbiol* 56(6):1919–1925.
85. Lücker S, et al. (2007) Improved 16S rRNA-targeted probe set for analysis of sulfate-reducing bacteria by fluorescence in situ hybridization. *J Microbiol Methods* 69(3): 523–528.
86. Manz W, Amann R, Ludwig W, Wagner M, Schleifer KH (1992) Phylogenetic oligodeoxynucleotide probes for the major subclasses of proteobacteria—Problems and solutions. *Syst Appl Microbiol* 15(4):593–600.
87. Loy A, et al. (2008) probeCheck—A central resource for evaluating oligonucleotide probe coverage and specificity. *Environ Microbiol* 10(10):2894–2898.
88. Wallner G, Amann R, Beisker W (1993) Optimizing fluorescent *in situ* hybridization with rRNA-targeted oligonucleotide probes for flow cytometric identification of microorganisms. *Cytometry* 14(2):136–143.
89. Caporaso JG, et al. (2010) QIIME allows analysis of high-throughput community sequencing data. *Nat Methods* 7(5):335–336.
90. Mason OU, et al. (2015) Comparison of archaeal and bacterial diversity in methane seep carbonate nodules and host sediments, Eel River Basin and Hydrate Ridge, USA. *Microb Ecol* 70(3):766–784.
91. Edgar RC (2010) Search and clustering orders of magnitude faster than BLAST. *Bioinformatics* 26(19):2460–2461.
92. Wang Q, Garrity GM, Tiedje JM, Cole JR (2007) Naive Bayesian classifier for rapid assignment of rRNA sequences into the new bacterial taxonomy. *Appl Environ Microbiol* 73(16):5261–5267.
93. Pruesse E, et al. (2007) SILVA: A comprehensive online resource for quality checked and aligned ribosomal RNA sequence data compatible with ARB. *Nucleic Acids Res* 35(21):7188–7196.
94. Quast C, et al. (2013) The SILVA ribosomal RNA gene database project: Improved data processing and web-based tools. *Nucleic Acids Res* 41(Database issue, D1):D590–D596.
95. Salter SJ, et al. (2014) Reagent and laboratory contamination can critically impact sequence-based microbiome analyses. *BMC Biol* 12:87.
96. Ludwig W, et al. (2004) ARB: A software environment for sequence data. *Nucleic Acids Res* 32(4):1363–1371.

Supporting Information

Hatzenpichler et al. 10.1073/pnas.1603757113

SI Text

SI Results and Discussion

Factors Limiting the Absolute Quantification of Newly Synthesized Proteins. BONCAT has the theoretical potential to detect all de novo synthesized proteins that contain at least one Met, i.e., ~99% of proteins in an average archaeal and bacterial proteome. However, in practice, several factors reduce this sensitivity and prohibit the absolute quantification of the amount of new protein, and, in consequence, of cell doubling times, from fluorescence data. (*i*) The process(es) by which HPG enters the cell is currently unknown and might depend on the physiological state of the cell or differ between different taxonomic groups; (*ii*) the rate at which HPG substitutes Met during protein synthesis has, so far, only been studied for *E. coli* (17) and might deviate in other organisms; (*iii*) due to varying contents of Met and contrasting copy numbers of proteins, distinct peptides contribute differently to overall fluorescence; and (*iv*) the extent by which protein recycling and posttranslational modification affect the stability of HPG (in particular its alkyne group) is currently unknown.

CARD-FISH vs. FISH. Our CARD-FISH experiments revealed marked discrepancies in the efficiencies to permeabilize and fluorescently detect different ANME subgroups. Most importantly, although ANME-1 constituted only 0.6% of all taxonomically identified consortia in our FISH experiments on sample #3730 (114 d sample; n = 167 consortia), the same subgroup represented 81.3% of detected ANME consortia in our CARD-FISH dataset (n = 48) (Table 1). This result is mainly explained by the inability of the used CARD-FISH protocol to detect ANME-2a and -2c consortia in our samples. This finding is in contrast to two recent studies that used near-identical permeabilization protocols for the successful visualization of these ANME groups in other methane seep sediments (36, 63).

Comparing ANME Community Structure in Sediment #3730 to Previous Studies. The very low proportion of aggregated ANME-1 in our Hydrate Ridge sediment (#3730) is consistent with a previous study on this methane seep, which found that ANME-1 occurred mostly as planktonic cells rather than in multicellular associations (26, 37). Because of our focus on syntrophic consortia in this study, we initially separated microbial aggregates of >3 μm from sediment particles. Planktonic ANME-1 cells thus might have partly evaded FISH detection. It should, however, be noted that our filtered samples contained large numbers of individual cells and that in no #3730 sample were individual cells found to bind the ANME-1-specific probe.

ANME-2a and -2c probes used in this study have been successfully used in previous mono-FISH studies of geographically distinct Hydrate Ridge sediment samples with hybridization rates of 20–80% of all DAPI-stained AOM consortia (37, 42). Because of the high spatial variance in ANME community structure (37, 38), it is, however, possible that our specific sediment samples hosted a unique combination of ANME clades. Alternatively, ANME community structure might have diverged from its original composition during the nearly 4 y of incubation in the laboratory before the experiments described herein were conducted.

Considerations on the Environmental Application of BONCAT. In contrast to the well-established stable isotope probing approach, the universal applicability of BONCAT is currently untested, and several questions demand rigorous investigation in future studies: (*i*) The mechanism(s) by which bioorthogonal amino acids are taken up by cells is currently unknown. If active transporters are required for their uptake, their absence would prohibit the application of BONCAT to that particular cell. To that effect, the recent report of up to 100% BONCAT labeling efficiency of planktonic microbes in surface seawater is encouraging (14). (*ii*) HPG and AHA, the bioorthogonal amino acids that have been used in environmental studies so far (refs. 9 and 14 and this study), have to compete with intracellular Met for incorporation into newly being made proteins. The preference of the translational machinery for Met over its synthetic surrogates (17) might therefore restrict the use of BONCAT in habitats featuring high concentrations of free Met. (*iii*) Lastly, substituting proteins with synthetic amino acids bears a high risk of interfering with the cellular machinery. We recently demonstrated that the addition of up to 1 mM of HPG or AHA had no detectable effect on the growth of several different, physiologically distinct archaeal and bacterial pure cultures for at least one cell generation. At longer incubation times, however, inhibition of growth could be observed at these high concentrations (9, 46). For environmental applications, we thus recommend that low concentrations of bioorthogonal amino acid should be used, incubation times be kept to a minimum, and complementary experiments testing for potential community shifts be performed (for details, see ref. 46).

SI Materials and Methods

Environmental Sampling and Storage. Sediment sample #3730 was obtained from Hydrate Ridge South methane seep field (R/V *Atlantis* cruise AT-15-68, Alvin Dive 4635; push-core 16; 44°34.09 N, 125°9.14 W; 775 m water depth; sediment horizon 0–6 cm; 4 °C in situ temperature) on 7 August 2010. Sediment was stored under argon headspace in a Mylar bag for 5 wk before being transferred to a 1-L glass bottle with a 1.38 bar 100% methane headspace, which was stored at 4 °C for ~4 y. Seawater and headspace were exchanged at regular intervals to prevent the accumulation of inhibitory compounds.

Sediment samples #7135 and #7136-37/37 were collected from Santa Monica Basin on 9 May 2013 (R/V *Western Flyer* MBARI Cruise 2013; dive 463; push-core 43; 33°47.34 N, 118°40.10 W; 860 m water depth; horizons 6–9 cm (#7135) and 9–15/15–22 cm (#7136-37/37, pooled) below a pink and white microbial mat; 4 °C). Sediment slurry was stored in a glass bottle for ~1 y under argon at 4 °C before BONCAT experiments were carried out.

Sediment sample #7142 was collected from Santa Monica Basin on 7 May 2013 (R/V *Western Flyer* MBARI Cruise 2013; dive 459; push-core 74; 33°47.34 N, 118°40.09 W; 863 m depth; sediment horizon 4–6 cm; 4 °C in situ temperature). The sediment was sealed under argon and stored at 4 °C. After 40 d of storage, the sediment was suspended in anaerobic natural bottom seawater from the site in an anaerobic chamber (3% H_2 in N_2) and aliquots were overpressured with 1.5 bar methane. The sediment was kept for 12 mo under 1.5 bar 100% methane in natural bottom seawater that was exchanged every 3 mo.

Sediment sample #5119 was collected from the Hydrate Ridge methane field during R/V *Atlantis* Cruise AT-18-10 on 1 September 2011 (44°40.02 N, 125°6.00 W; dive J2-593 E4A; push-core 36 through a yellow microbial mat; water depth 600 m; sediment horizon 9–12 cm). Sediment #5202 was collected during the same cruise on 3 September 2011, dive J2-593 E6B (44°40.02 N, 125°7.51 W; push-core 18 through a pink and white microbial mat; water depth 601 m; horizon 3–6 cm).

Carbonate #3439 was collected from atop an active seep at the Hydrate Ridge methane field during cruise AT-15-68 on 1 August 2010 (44°34.09 N, 125°9.14 W; dive AD4629; water depth 775 m). Carbonate sample #2450 was retrieved from sediment sample #2450 collected at Eel River Basin on 27 July 2005 (40°48.68 N, 124°36.73 W; dive T-864; push-core 49; horizon 0–2 cm; water depth 516 m).

Information on the geochemical characteristics of the sampling sites may be requested from the corresponding authors.

Setup of Incubations. All samples were kept in an ice bath at all times during handling. Artificial seawater (ASW) consisted of 10.9 g of $MgCl_2{\cdot}6H_2O$, 0.2 g of $NaHCO_3$, 0.76 g of KCl, 25.9 g of NaCl, 1.47 g of $CaCl_2{\cdot}2H_2O$, 3.98 g of Na_2SO_4, and 26.73 mg of NH_4Cl per liter of ddH_2O at pH 7.4. One milliliter of vitamin solution (see medium 141, https://www.dsmz.de) and 1 mL of trace element solution SL-10 (see https://www.dsmz.de) were also added. Before use, ASW was filtered through a 0.2-μm filter and N_2-bubbled for 10 min. ASW was kept on ice during handling.

Approximately 50 mL of wet sediment #3730 was resuspended in ASW, yielding a total volume of ∼130 mL; 20-mL aliquots of homogenized slurry were transferred into 160-mL serum bottles, and 30 mL of ASW was added. Bottles were sealed with rubber stoppers, and headspaces were flushed with either 100% methane or 100% N_2 for 5 min before being pressurized with 2 bar 100% methane or 100% N_2. Sediment was allowed to equilibrate overnight (∼18 h) at 4 °C in the dark; 0.2 μm-filtered HPG (Click Chemistry Tools) in ddH_2O was added to reach a final concentration of 50 μM. Control incubations without HPG were supplemented with sterile ddH_2O to reach equal volumes. All bottles were then flushed for 5 min, pressurized with 2 bar methane or N_2, and incubated in the dark at 4° C. In total, six incubations were performed: two times without HPG plus methane, two times with 50 μM HPG plus methane, and two times with 50 μM HPG plus N_2.

Approximately 100 mL of wet sediment #7135 was resuspended in ASW, yielding a total volume of ∼300 mL, and incubated for 15 d under 2 bar 100% methane. After this preincubation, 100 mL of ASW was added, and the slurry was homogenized. Under constant N_2 flushing, 35-mL aliquots were transferred into 160-mL serum bottles, bottles were sealed with rubber stoppers, and headspaces were flushed for 5 min with either 100% methane or 100% N_2, depending on incubation setup. HPG was added to reach a final concentration of either 5 μM or 50 μM. In addition, controls without HPG were supplemented with sterile ddH_2O to reach equal incubation volumes. Then, all bottles were flushed for 5 min, overpressurized with 2 bar methane or N_2, and incubated in the dark at 4 °C. In total, 12 incubations were performed: four times without HPG plus methane, four times with 50 μM HPG plus methane, two times with 50 μM HPG plus N_2, and two times with 5 μM HPG plus methane.

Twenty milliliters of wet sediment #7136-37 was resuspended in ASW, yielding a total volume of ∼50 mL. The slurry was bubbled with N_2 for 10 min (this was repeated after 5 d) before the bottle was incubated for 124 d under 2 bar N_2 (detectable but nonquantifiable amount of methane, 1–10 ppm). After this prestarving, 10-mL aliquots were transferred into 75-mL bottles. HPG was added to reach a final concentration of 50 μM, and 2 bar 100% methane or 100% N_2 (2 bar) was added to the headspace of two aliquots each. In addition, a control mesocosm was incubated without HPG under 100% methane (2 bar). All bottles were incubated at 4 °C in the dark for 31 d.

One-milliliter aliquots of wet sediment #7142 in 5 mL ASW containing 25 mM Hepes buffer (pH 7.5), 5 mM sulfide, and 5 mM DIC were resuspended in serum vials, which were then sealed with rubber stoppers (12.9 mL final volume). The headspace was flushed with $^{12}CH_4$ before 1.0 mL $^{13}CH_4$ (99% ^{13}C, containing 0.05 vol% $^{13}CO_2$ as impurity; Cambridge Isotope Laboratories) was added. After ∼5 d of preincubation, HPG was added to two of the four bottles to reach a concentration of 50 μM. In addition, one incubation was performed at 250 μM HPG for 25 d and later used for activity-based cell sorting.

Sampling for Molecular and Geochemical Analyses. Sampling of sediment microcosms was undertaken at incubation start as well as after 30 d, 73 d, and 114 d and 7 d, 14 d, 41 d, 56 d, and 171 d for sediment #3730 and #7135, respectively. Samples for molecular, cellular, and geochemical analyses were removed using sterile syringes while the incubation bottles were kept in an ice bath.

At each sampling point, 0.25 mL of sediment slurry was transferred into a sterile 1.5-mL tube and centrifuged at 16,100 g for 10 s at RT. The supernatant (SN) was removed, mixed in a 1:1 ratio with 0.5 M Zn-acetate solution, and stored for later sulfide analysis. The pellet was flash-frozen using liquid N_2 and stored at −20 °C for DNA extraction; 0.25 mL of sediment slurry was removed, centrifuged as described above, the SN was wasted, and the pellet was resuspended in a 1:1 mix of 1× PBS and absolute ethanol. Another 0.25 mL was processed in the same way but resuspended in 3% paraformaldehyde (PFA; Electron Microscopy Sciences) in 1× PBS and incubated for 1 h at RT for chemical fixation of cells. Afterward, biomass was harvested by centrifugation, the SN was wasted, and the pellet was washed with 1.5 mL of 1× PBS. Finally, sediment was centrifuged, the SN was wasted, and the biomass was resuspended in a 1:1 mix of 1× PBS and ethanol. All ethanol- or PFA-fixed samples were kept at −20 °C until further processing. After sampling (30 d, 73 d, and 114 d and 7 d, 14 d, 41 d, 56 d, and 171 d for #3730 and #7135, respectively), the headspace of bottles was flushed for 3 min with either methane or N_2 before the sediment was again incubated at 4 °C with 2 bar of either 100% methane or 100% N_2, depending on incubation setup. In addition, after 73 d (#3730) and 41 d and 130 d (#7135), ∼90% of artificial seawater overlying sediment was exchanged. The slurry volume and sediment-to-water ratio of all incubations was identical at all times for each sediment type (#3730 or #7135, respectively). When appropriate, newly added seawater was then supplemented with 5 μM or 50 μM (final) HPG.

Geochemical Analyses. Sulfide (H_2S plus HS^-) concentrations were determined via the cline assay (82). Samples were analyzed for statistically relevant differences via Student's t test. Differences were considered to be significant at $P \leq 0.05$. Methane oxidation rates for sediment #7142 were determined as described by Scheller et al. (29) by measuring the formation of DIC from $^{13}CH_4$ over time. Succinctly, 0.25 mL of ASW overlying settled sediment was removed and centrifuged (16,000 × g for 5 min). The SN was transferred into 0.6-mL tubes, flash frozen in N_2, and stored at −20 °C until further processing; 150 μL of thawed SN was then added to He-flushed vials containing 100 μL H_3PO_4 (85%). The resulting CO_2 was analyzed for isotopic enrichment on a GC-IR-MS GasBench II (Thermo Scientific).

Extraction of Microbial Aggregates. To separate microbial aggregations and individual cells from sediment particles, 50 μL of sediment slurry was resuspended in 450 μL of 1× PBS in a 2-mL tube. This solution was chilled in an ice bath for 15 min before being sonicated three times for 10 s at 3–6 W output using a Branson Sonifier 150 (Branson Ultrasonics Corporation). Between pulsing intervals, the sample was allowed to cool for 10–30 s. After sonication, the sample was applied on top of 500 μL Percoll (Sigma-Aldrich) and centrifuged at 16,100 × g for 20 min at 4 °C. To remove Percoll particles and the majority of individual planktonic cells, the entire SN was resuspended in 15 mL 1× PBS and filtered through a 3-μm TSTP white polycarbonate filter (EMD Millipore) using a filter tower at ∼0.3 bar under pressure. Each filter was washed with a total volume of 50 mL 1× PBS without letting the filter run dry. Then, particles and biomass that had been retained by the filter were transferred into a 2-mL tube using 1× PBS by repeatedly and vigorously pipetting up and down using a 1-mL

pipette. DAPI staining confirmed that this protocol leads to the near-complete transfer of microbial aggregates from the filter into solution (99–100% of DAPI-stained consortia), without selecting for or against a particular type of consortium morphology or size. After transfer into 1× PBS, biomass was harvested via centrifugation (16,100 × *g*, RT), resuspended in either 1× PBS (for nonfixed BONCAT analyses) or a 1:1 ratio of 1× PBS and ethanol (fixed biomass), and stored at either 4 °C (nonfixed) or −20 °C (fixed).

List of Oligonucleotide Probes for FISH and CARD-FISH. In FISH experiments, monolabeled and dual-labeled (indicated with ** in the list below) probes were used in different combinations (Dataset S2): Arch915, specific for most members of the domain *Archaea* (83), used at 35% formamide (FA); EUB338, -II, and -III (also known as EUB338mix), which together cover most of the known bacterial diversity (72, 84), used at 35% FA; EUB338-III, specific for most members of the *Verrucomicrobia* (72), used at 35% FA, in combination with EUB338-I and -II as competitor probes; Delta495a** together with its competitor probe, specific for most delta-proteobacteria (85), used at 35% FA; Gam42a, together with its competitor, specific for most gamma-proteobacteria (86), used at 35% FA; Ver47**, specific for *Verrucomicrobia* (73) together with its helper probe H64 (74) at 15% FA; and ANME-1-350 (26) (40% FA), ANME-2-932 (also known as EelMS-932; 26) (40% FA), ANME-2a-647 (50% FA) (37), and ANME-2c-760** (60% FA) (37), specific for different subpopulations of ANME. In addition, a new probe, ANME-2b-729, was designed, which detects >93% of all ANME-2b-affiliated 16S rRNA sequences in online and laboratory internal databases. The new probe has at least two mismatches to all other archaeal or bacterial 16S rRNA sequences [tested using probeCheck (87)]. After careful evaluation, ANME-2b-729 was used at 20% formamide concentration. Note that this probe has a one-nucleotide overlap with probe ANME-2-712 (37) and should thus not be used in conjunction with this probe. Hybridizations without probe addition or probe NONEUB388 (88) were used as negative controls.

With the exception of probe ANME-2a-647, which was used at 40% FA (rather than 50%), all probes used in CARD-FISH were used at the same FA concentrations as in FISH experiments. For CARD-FISH, hybridizations with probe NONEUB388 were used as negative controls.

Multiple Displacement Amplification. Individual sorted consortia were lysed and subjected to WGA as previously described (65) with the following modifications: WGA was performed with a REPLI-g Single Cell Kit (Qiagen) with a scaled-down reaction volume of 2 μL and DNA dye SYTO-13 added at 1× for real-time tracking. The cell lysis procedure followed a recently described protocol (65), which was modified by lysozyme treatment. This step included a 15-min RT incubation with 300 nL of 50 U/μL ReadyLyse lysozyme (Epicentre R1810M), which was followed by the addition of 50 nL concentrated DLB buffer (65). Lysis and stop reagents were UV-treated as described (65), and the Master Mix was used as obtained from the manufacturer (Qiagen). The amplification reaction was incubated for 6 h at 30 °C.

The 16S rRNA Gene Tag Sequencing. Sediment DNA was extracted using the Power Soil DNA Isolation Kit according to the manufacturer's protocol (MoBio), and diluted DNA from genome-amplified sorted consortia was used directly. The V4 region of the 16S rRNA gene was amplified from each extract using archaeal and bacterial primers 515F (GTGCCAGCMGCCGCGGTAA) and 806R (GGACTACHVGGGTWTCTAAT) (67, 68). Sediment samples were amplified in duplicate. The nonbarcoded primers were used with Q5 Hot Start High-Fidelity 2× Master Mix (New England Biolabs) according to the manufacturer's directions, using annealing conditions of 54 °C for 30 cycles and 58 °C for 32 cycles for sediments and MDAs, respectively. Duplicates of sediment sample amplifications were then pooled. The barcoded 806R primer (CAAGCAGAAGACGGCATACGAGAT XXXXXXXXXXXX AGTCAGTCAG CC GGACTACHVGGGTWTCTAAT) was paired with 515F in a reconditioning reaction (same conditions as above except for five cycles of PCR) to barcode the PCR products. Samples were mixed together in equimolar amounts and purified in bulk through a Qiagen PCR purification kit before submission to Laragen for analysis on an Illumnia MiSeq platform. The resulting paired-end sequence data, 2× 250 bp, was demultiplexed, and sequences with >1 bp mismatch on the 12-bp barcode were removed. The resulting sequences were passed through Illumina's MiSeq Recorder software to assign quality scores to each base call and remove adapter, barcode, and primer sequence.

Analysis of 16S rRNA Gene Tag Sequences. Sequence data were processed in QIIME (Quantitative Insights Into Microbial Ecology) version 1.8.0 (89) following a recently published protocol (90). Raw sequence pairs were joined and quality-trimmed using the default parameters in QIIME. Sequences were clustered into de novo OTUs with 99% similarity using UCLUST open reference clustering protocol (91). Then, the most abundant sequence was chosen as representative for each de novo OTU (92). Taxonomic identification for each representative sequence was assigned using the SILVA-115 database (93, 94) clustered at 99% similarity. This SILVA database had been appended with 1,197 in-house high-quality, methane-seep derived bacterial and archaeal clones. Any sequences with pintail values >75 were removed. The modified SILVA database is available upon request from the corresponding authors. OTUs were then filtered to remove singletons from the combined MDA dataset. A threshold filter was used to remove any OTU that occurred below 0.01% of the entire combined sediment samples dataset. Known contaminants in PCR reagents as determined by the analysis of negative and positive controls run with each MiSeq set were also removed (95). For the sediment samples, the sequence data were rarified by random subsampling to equal the sample with the least amount of sequence data, resulting in 12,115 and 3,707 sequences per sample for sediments #3730 and #7135, respectively. Tables of both absolute and relative abundances were generated at the family level for each sample. For statistical and similarity percentage analyses [Nonmetric Multidimensional Scaling (NMDS), Analysis of Similarity (ANOSIM), and Similarity Percentage], family-level abundance tables were square-root-transformed before generation of Bray Curtis similarity matrices and analyzed using Primer-E software (www.primer-e.com). Differences were considered to be significant at $P \leq 0.05$.

Phylogenetic Analysis. The 16S rRNA gene tag sequences from each consortium as well as closely related sequences from online databases (identified via the BLAST algorithm of National Center for Biotechnology Information) were imported into and analyzed via the ARB software package (96). Sequences were automatically aligned to reference sequences of all ANME subpopulations as well as relevant bacterial clades contained within the SILVA-115 database that had been amended with 1,197 in-house seep derived clones. Sequences from cultured representatives of archaeal phyla *Thaumarchaeota* and *Euryarchaeota* were used as outgroup for reconstruction of the archaeal tree. Members of the *Planctomycetes* where chosen as outgroup for the bacterial tree. Both alignments were manually curated, and termini filters were created. During the phylogenetic reconstruction of archaeal (all >1,100 nt in length) and bacterial (all >1,000 nt in length) sequences, 958 and 1,255 positions were considered, respectively. Phylogenies were modeled using a Randomized Axelerated Maximum Likelihood (RaxML) algorithm, and short tag sequences were individually added to the resulting tree using the parsimony interactive tool in ARB without changing the overall topology of the tree. In addition, maximum parsimony (100× replications) and Neighbor Joining (1,000× replications) trees were calculated, and bootstrap values were projected onto the RaxML tree.

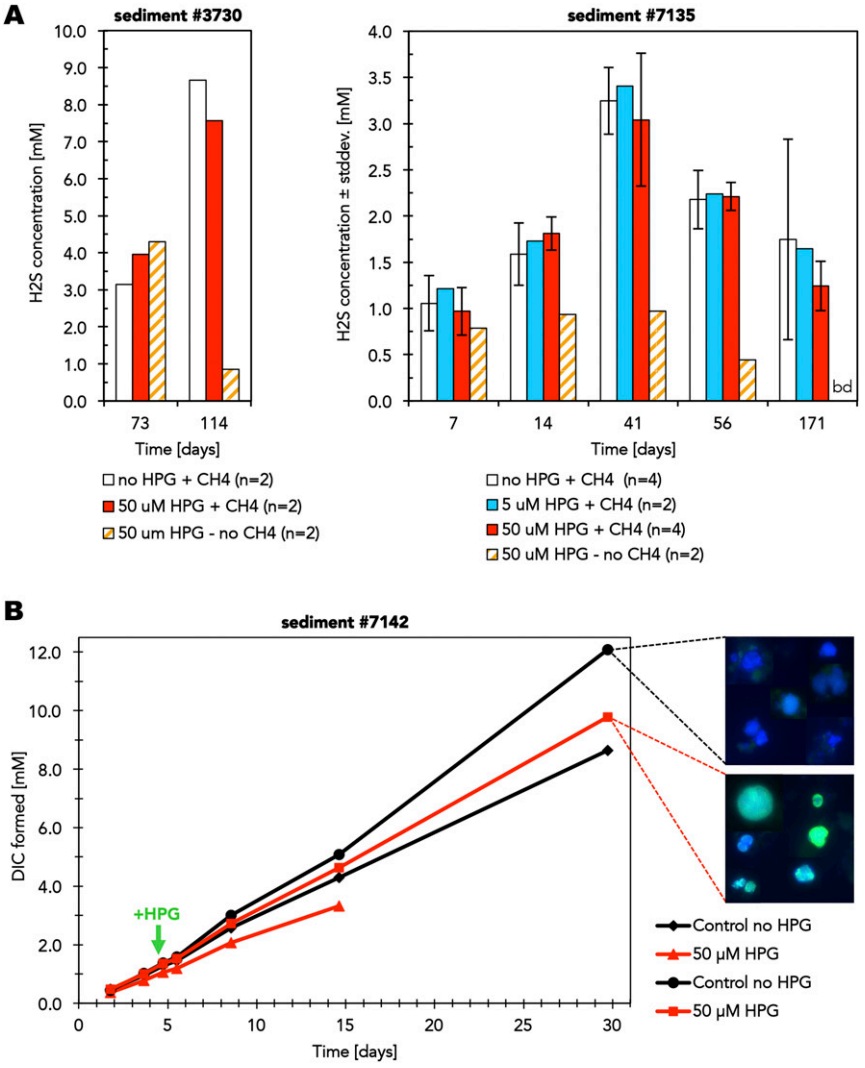

Fig. S1. Sediment sulfide production rates and methane oxidation rates are not affected by the presence of HPG. (*A*) Sulfide [H_2S + HS^-] levels cannot be directly compared between different time points, because seawater and headspace of incubations were refreshed at regular intervals. In contrast to HPG, methane has a statistically significant effect on sulfide production ($P = 0.0183$ and $P = 0.0063$ for #3730 and #7135 after 114 d and 56 d of incubation, respectively). Sulfide levels in sediment #7135 samples #09 and #10 (both without methane) were below detection limit (bd) after 171 d of incubation. (*B*) Sediment methane oxidation rates are not affected by the presence of HPG over a course of up to 25 d. Four separate aliquots of sediment #7142 were incubated in the absence of HPG for ∼5 d, after which 50 µM HPG (final concentration) was added to two incubations. Note that one of the HPG-containing incubations exhibited low rates of AOM from the start of the experiment on. Because of this, the experiment was stopped after ∼10 d of incubation. Compilations of representative AOM consortia from the endpoints of two incubations are shown on the right. Green fluorescence indicates that cells have been translationally active during time of incubation. DAPI-stained DNA is in blue. Methane oxidation rates were measured as ^{13}C DIC formed from $^{13}CH_4$. Sampling on day 5 was performed immediately after addition of HPG.

A

3730			HPG	NO	NO	NO	50	50	50	50
			CH4	Y	Y	Y	Y	Y	NO	NO
			Time	0	114	114	114	114	114	114
HPG	CH4	Time	Sample	#0	#1	#2	#3	#4	#5	#6
NO	Y	0	#0							
NO	Y	114	#1	91.7						
NO	Y	114	#2	92.0	94.5					
50	Y	114	#3	90.8	94.3	94.2				
50	Y	114	#4	91.0	94.4	93.1	94.8			
50	NO	114	#5	88.4	92.6	91.8	93.2	92.2		
50	NO	114	#6	91.1	93.6	92.8	93.6	92.7	92.8	

NO no HPG addition
5 5 μM HPG
50 50 μM HPG
HPG

NO 30 psi N2
Y 30 psi CH4
CH4

3730: 12,115 sequences
7135: 3,707 sequences

Bray Curtis similarity [%]
85.7 94.8

0 start
114 114 days
41 41 days
171 171 days
Time

B

7135			HPG	NO	NO	NO	NO	NO	NO	NO	NO	50	50	50	50	50	50	50	50	50	50	50	50	5	5	5	5
			CH4	Y	Y	Y	Y	Y	Y	Y	Y	Y	Y	Y	Y	Y	Y	Y	Y	NO	NO	NO	NO	Y	Y	Y	Y
			Time	41	41	41	41	171	171	171	171	41	41	41	41	171	171	171	171	41	41	171	171	41	41	171	171
HPG	CH4	Time	Sample	#01	#02	#03	#04	#01	#02	#03	#04	#05	#06	#07	#08	#05	#06	#07	#08	#09	#10	#09	#10	#11	#12	#11	#12
NO	Y	41	#01																								
NO	Y	41	#02	92.7																							
NO	Y	41	#03	92.9	92.3																						
NO	Y	41	#04	91.2	91.9	91.8																					
NO	Y	171	#01	87.9	88.2	87.7	88.5																				
NO	Y	171	#02	87.3	87.8	89.0	87.6	86.6																			
NO	Y	171	#03	87.6	88.2	87.7	88.1	91.2	88.9																		
NO	Y	171	#04	87.1	88.2	88.1	87.3	89.9	87.3	90.1																	
50	Y	41	#05	91.8	91.4	92.3	90.7	87.8	88.3	87.2	87.1																
50	Y	41	#06	92.1	92.2	93.7	90.9	87.6	89.2	87.7	87.9	90.7															
50	Y	41	#07	93.4	92.4	92.6	92.3	87.9	87.0	87.6	87.5	91.3	92.8														
50	Y	41	#08	90.9	92.7	92.5	91.7	88.8	88.8	88.5	88.7	91.4	91.5	91.6													
50	Y	171	#05	89.3	88.9	89.2	88.6	89.9	88.0	89.6	88.4	88.5	88.7	89.4	88.4												
50	Y	171	#06	88.8	89.0	89.3	88.5	90.3	87.3	90.8	90.0	87.5	88.8	88.5	88.9	90.7											
50	Y	171	#07	90.0	91.0	90.4	89.4	90.3	87.5	89.7	89.8	89.5	89.5	89.2	89.9	89.7	89.8										
50	Y	171	#08	89.9	90.6	90.5	89.6	89.2	89.8	89.1	88.8	90.9	90.3	90.5	90.4	90.9	89.1	90.1									
50	NO	41	#09	89.9	89.3	90.2	90.4	86.7	85.7	88.6	86.7	89.0	87.9	88.7	90.1	87.4	88.3	89.9	87.4								
50	NO	41	#10	91.3	91.8	92.1	89.8	86.8	89.1	86.4	86.2	90.8	91.6	91.0	91.3	88.1	87.8	89.4	90.7	89.2							
50	NO	171	#09	89.3	89.9	88.8	88.1	89.4	87.7	88.9	88.4	88.1	88.2	88.6	88.3	90.5	89.0	90.5	90.1	88.4	88.5						
50	NO	171	#10	89.2	88.9	89.3	88.2	89.4	86.8	88.8	88.9	88.0	87.7	88.7	89.0	89.0	89.5	91.2	88.5	89.4	88.3	90.4					
5	Y	41	#11	91.0	92.1	91.9	90.8	88.1	88.5	88.2	86.5	90.2	90.6	90.8	91.3	87.5	88.7	89.5	89.1	89.8	90.8	88.5	88.4				
5	Y	41	#12	92.6	92.8	93.2	92.2	88.0	88.0	88.3	87.0	92.2	91.2	92.2	91.8	89.6	88.8	90.6	89.7	91.1	91.4	88.7	89.0	91.8			
5	Y	171	#11	88.5	88.5	90.4	89.9	86.5	87.5	86.6	86.0	89.4	89.2	88.7	88.8	87.9	86.7	90.1	89.8	88.7	88.4	86.8	87.1	88.3	89.3		
5	Y	171	#12	89.4	90.1	89.6	89.6	90.9	87.9	91.2	90.7	89.1	89.3	89.3	90.2	89.0	91.1	90.1	90.2	89.1	89.6	89.6	89.5	89.3	89.2	87.2	

Fig. S2. Bray Curtis similarity indexes of the microbial communities of sediments #3730 (*A*) and #7135 (*B*) after incubation in the absence or presence of HPG for 114 d and 171 d, respectively. For statistical analyses, see Figs. S3 and S4.

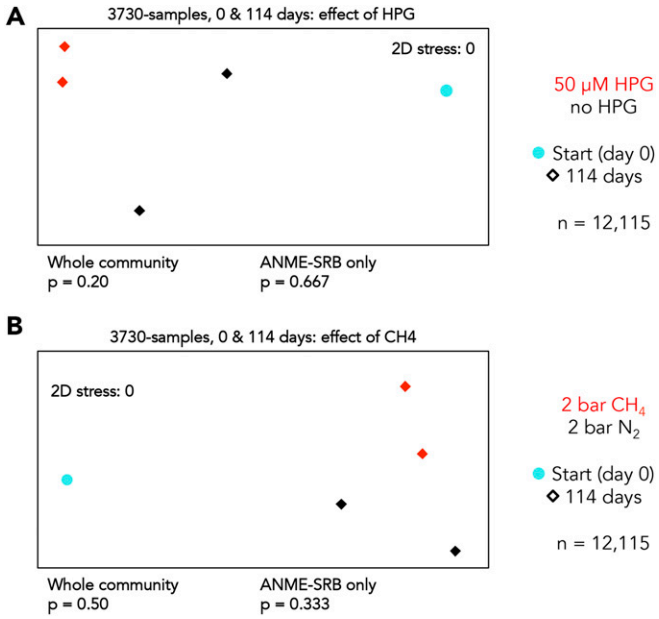

Fig. S3. NMDS ordinations of 16S rRNA gene tag sequences demonstrated that neither HPG (*A*) nor methane (*B*) have a statistically relevant effect on the microbial community of sediment #3730 after 114 d of incubation. Stress values of NMDS ordinations and *P* values of concomitant Anosim analyses for whole communities and ANME–SRB-related lineages specifically are shown next to the plots; n, number of sequences per sample. The more similar the microbial communities from two samples are, the closer they lie together. Differences between samples were considered to be significant at $P \leq 0.05$.

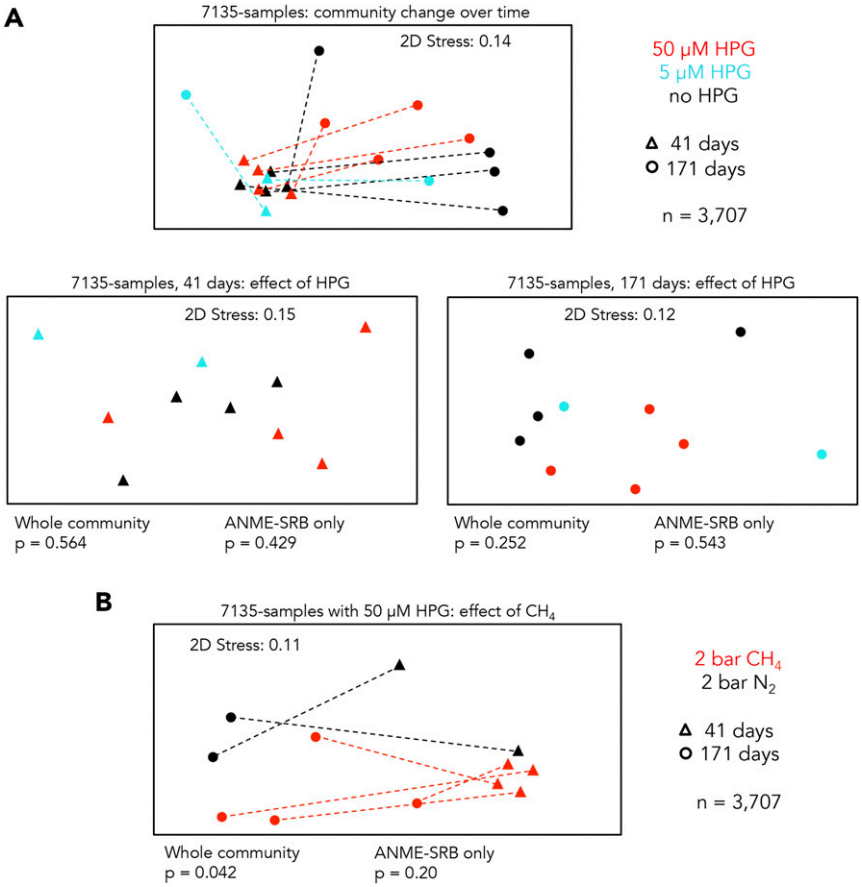

Fig. S4. (*A*) NMDS ordinations of 16S rRNA gene tag sequences demonstrated that HPG does not have a statistically relevant effect on the microbial community of sediment #7135 after 171 d of incubation. (*B*) The absence of methane, on the other hand, has a clear effect on the community composition. Stress values of NMDS ordinations and *P* values of concomitant Anosim analyses for whole communities and ANME–SRB-related lineages specifically are shown next to the plots. Dotted lines connect the individual sampling points for each incubation bottle; n, number of sequences per sample. The more similar the microbial communities from two samples are, the closer they lie together. Differences between samples were considered to be significant at $P \leq 0.05$.

A

3730	HPG	NO	NO	NO	50	50	50	50
	CH4	Y	Y	Y	Y	Y	NO	NO
	TIME	0	114	114	114	114	114	114
	Sample	#0	#1	#2	#3	#4	#5	#6
ANME-1;Other		0.7	0.3	0.4	0.4	0.4	0.2	0.3
ANME-1;ANME-1a		20.3	14.6	15.0	12.8	15.7	9.8	12.4
ANME-1;ANME-1b		1.3	1.2	1.5	1.5	0.9	1.0	0.9
Methanosarcinales;ANME-2a-2b		9.7	6.0	7.9	6.1	5.2	4.5	6.5
Methanosarcinales;ANME-2c		6.1	5.8	5.0	6.9	7.0	4.2	5.6
Methanosarcinales;Methanosaetaceae		0.0	0.0	0.0	0.1	0.0	0.0	0.0
Desulfarculales;Desulfarculaceae		0.4	0.9	0.6	0.9	0.8	1.0	0.8
Desulfobacterales;Desulfobacteraceae		11.9	12.5	10.7	10.8	11.6	14.4	16.8
Desulfobacterales;Desulfobulbaceae		3.3	4.4	5.0	4.5	4.3	5.1	4.8
Desulfuromonadales;Desulfuromonadaceae		0.2	0.2	0.5	0.3	0.3	0.5	0.2
Other archaea		0.9	1.1	1.0	1.0	1.2	1.4	0.7
Other bacteria		45.1	52.9	52.3	54.7	52.6	58.0	50.9

3730: 12,115 sequences

7135: 3,707 sequences

Relative abundance of taxon [%]

low — high

HPG
- NO no HPG addition
- 5 5 μM HPG
- 50 50 μM HPG

CH4
- NO 30 psi N2
- Y 30 psi CH4

Time
- 0 start
- 114 114 days
- 41 41 days
- 171 171 days

B

7135	HPG	NO	NO	NO	NO	NO	NO	NO	NO	50	50	50	50	50	50	50	50	50	50	50	50	5	5	5	5
	CH4	Y	Y	Y	Y	Y	Y	Y	Y	Y	Y	Y	Y	Y	Y	Y	Y	NO	NO	NO	NO	Y	Y	Y	Y
	Time	41	41	41	41	171	171	171	171	41	41	41	41	171	171	171	171	41	41	171	171	41	41	171	171
	Sample	#01	#02	#03	#04	#01	#02	#03	#04	#05	#06	#07	#08	#05	#06	#07	#08	#09	#10	#09	#10	#11	#12	#11	#12
ANME-1;_ANME-1a		2.3	1.7	1.9	4.2	3.2	1.3	2.1	5.4	3.3	2.8	3.4	1.8	3.3	2.1	1.5	3.6	0.7	1.6	1.5	1.2	1.2	1.9	2.6	2.4
ANME-1;_ANME-1b		0.3	0.2	0.3	0.2	0.1	0.0	0.1	0.1	0.3	0.1	0.2	0.1	0.1	0.0	0.1	0.1	0.1	0.1	0.1	0.2	0.2	0.1	0.2	0.2
Methanomicrobia;D-C06;__f		0.0	0.0	0.0	0.0	0.0	0.0	0.0	0.0	0.0	0.0	0.0	0.2	0.0	0.1	0.0	0.0	0.0	0.1	0.0	0.0	1.1	0.0	0.0	0.1
Methanosarcinales;ANME-2a-2b		0.7	0.7	0.9	0.7	1.3	0.5	1.5	1.0	0.4	0.8	0.5	0.9	0.6	1.4	0.8	0.5	0.3	0.2	0.3	0.4	0.7	0.5	0.7	1.1
Methanosarcinales;ANME-2c		1.1	1.8	1.4	1.6	4.9	7.8	7.5	3.4	1.5	2.0	1.2	1.7	3.0	4.8	2.4	3.3	0.4	0.6	2.1	1.3	1.1	0.8	1.8	3.5
Desulfarculales;Desulfarculaceae		1.1	0.9	1.0	0.9	0.8	1.0	0.9	0.9	1.0	1.1	0.8	0.9	0.9	1.0	1.2	1.2	1.5	1.0	0.9	1.2	0.9	1.1	2.0	0.9
Desulfobacterales;Desulfobacteraceae		3.3	3.5	3.4	3.4	4.4	6.0	5.9	5.8	3.8	3.2	3.3	3.4	4.7	4.3	5.6	4.3	4.9	4.4	4.5	3.5	3.6	3.6	6.8	5.2
Desulfobacterales;Desulfobulbaceae		3.2	2.8	2.8	2.8	2.8	2.6	2.3	2.3	2.5	3.0	3.3	2.6	2.2	3.0	2.9	2.9	2.4	3.3	2.1	2.0	2.6	2.6	3.2	2.9
Other archaea		13.6	14.1	12.8	12.8	14.2	9.1	11.9	12.6	13.2	11.3	12.8	13.7	12.1	12.3	13.3	12.2	12.8	11.7	17.3	17.1	12.1	12.0	9.6	12.4
Other bacteria		74.3	74.2	75.2	73.3	68.2	71.5	67.5	68.2	73.9	75.5	74.2	74.6	72.8	70.8	72.0	71.7	76.6	76.7	71.1	72.8	76.2	77.3	73.1	71.3

Fig. S5. Relative abundances of ANME-related archaea and SRB in sediment #3730 (*A*) or #7135 (*B*) over time. Abundance-based color-coding indicates relative abundance of taxa within a sample. Sequences summarized as "other archaea," which are slightly enriched in #7135 samples incubated in the absence of methane, were related to rRNA genes from Marine Benthic Group D/Deep Sea Hydrothermal Vent Euryarchaeotal Group 1 as well as the Marine Hydrothermal Vent Group and Miscellaneous Euryarchaeotal Group. The physiology of these uncultured, yet environmentally widely distributed, clades is currently unknown. However, recent genomic data suggest an implication of members of Marine Benthic Group D in the degradation of detrital proteins in marine sediments.

Fig. S6. Extended versions of the phylogenetic trees shown in Fig. 5. Green and white colored boxes in trees show support ≥90% and ≥70%, respectively. Values <70% are not given. Boxes in left and right trees indicate maximum parsimony (100×) and neighbor joining (1,000×) values, respectively. Numbers in boxes give the number of sequences within a group. The 16S rRNA gene tag sequences were added after tree construction without changing overall tree topology. Dotted lines indicate individual partnerships. The scales bars represent 10% estimated sequence divergence.

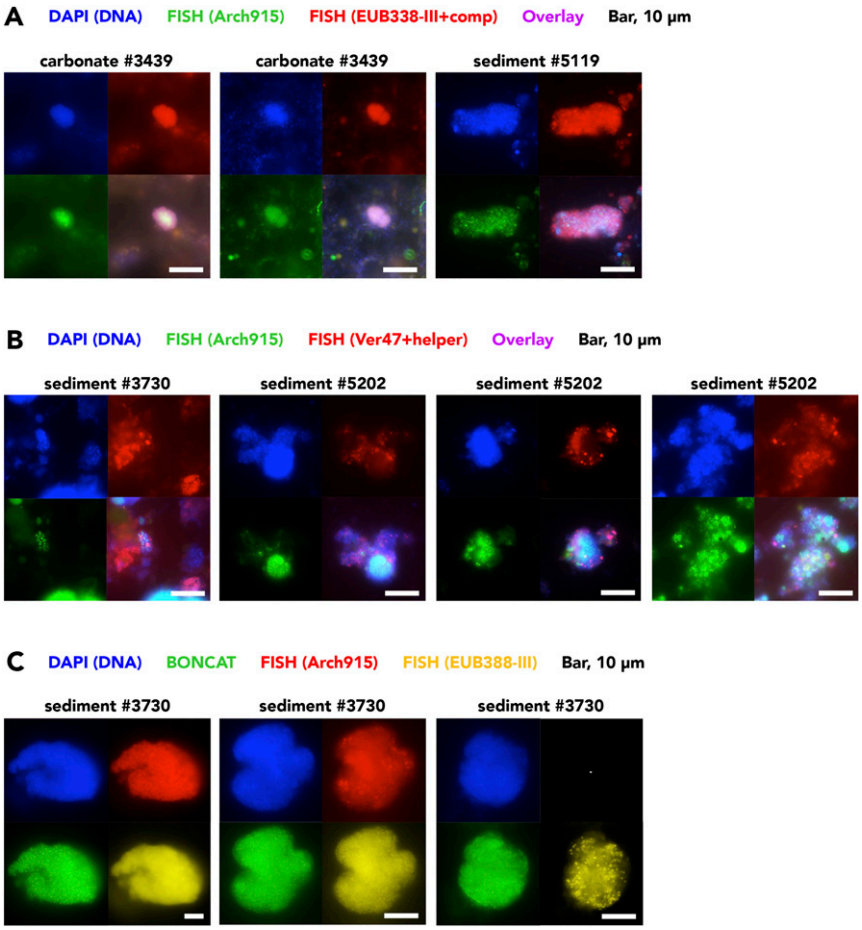

Fig. S7. Representative images of our FISH-based screening of methane seep sediment and carbonate samples for associations of *Archaea* and members of the *Verrucomicrobia*. *A–C* show results of screenings using different combinations of *Archaea*- and *Verrucomicrobia*-targeted FISH probes. For references of FISH probes and detailed aggregate-counts for specific samples refer to *SI Text* and Dataset S3. Arch915, a probe specific for archaea; EUB338-III, a probe specific for most *Verrucomicrobia*; comp, unlabeled competitor probes EUB338-I and II; Ver47, a *Verrucomicrobia*-specific probe, used together with an unlabeled helper probe (helper).

Dataset S1. Incubation setup and sampling details

Dataset S1

-, not determined; d, days of incubation; Y, yes; 5/50, 5/50 μM HPG.

Dataset S2. Details on BONCAT-FISH and FISH experiments summarized in Fig. 2

Dataset S2

For each probe set listed, the first probe had been labeled with a Cy3 dye, the second with a Cy5 dye. >, transfer to; comp, competitor probe; d, days of incubation; help, helper probe; na, not applicable; nd, not determined.

Dataset S3. Details on *Verrucomicrobia* FISH experiments

Dataset S3

For each probe set listed, the first probe had been labeled with a Cy3 dye, the second with a Cy5 dye. comp, competitor probe; cons, consortium/consortia; help, helper probe.